Journal of Ophthalmology

Application of Optical Coherence Tomography Angiography to Retinal Disease

Lead Guest Editor: Talisa E. De Carlo
Guest Editors: Nadia K. Waheed, Jayanth Sridhar, and Daniela Ferrara

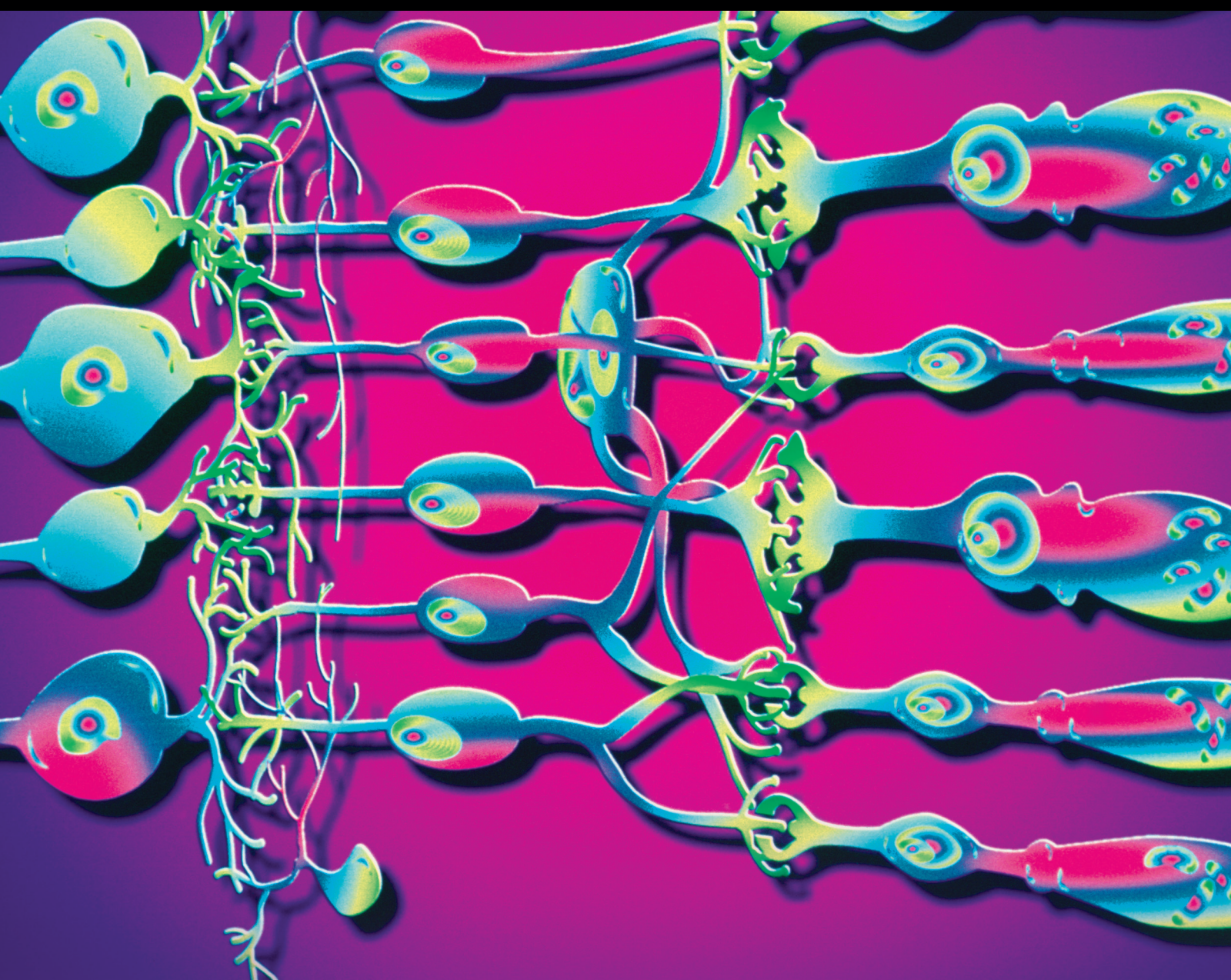

Application of Optical Coherence Tomography Angiography to Retinal Disease

Journal of Ophthalmology

Application of Optical Coherence Tomography Angiography to Retinal Disease

Lead Guest Editor: Talisa E. De Carlo
Guest Editors: Nadia K. Waheed, Jayanth Sridhar, and Daniela Ferrara

Editorial Board

Contents

Hindawi
Journal of Ophthalmology
Volume 2018, Article ID 5490592, 2 pages
https://doi.org/10.1155/2018/5490592

Editorial

Application of Optical Coherence Tomography Angiography to Retinal Disease

Talisa E. de Carlo,[1] **Nadia K. Waheed**,[2] **Jayanth Sridhar**,[3] **and Daniela Ferrara**[2]

[1]*Illinois Eye and Ear Infirmary, University of Illinois at Chicago, Chicago, IL, USA*
[2]*New England Eye Center, Tufts University School of Medicine, Boston, MA, USA*
[3]*Bascom Palmer Eye Institute, University of Miami, Miami, FL, USA*

Correspondence should be addressed to Talisa E. de Carlo; talisa.e.decarlo@gmail.com

Received 14 January 2018; Accepted 15 January 2018; Published 7 August 2018

A little over two years ago, a hot new topic in retinal imaging caught the attention of ophthalmologists around the world. Optical coherence tomography angiography (OCTA), an innovative, fast, noninvasive, non-dye-based angiographic technique, quickly became a topic of great interest in major conferences and ophthalmology journals. Inquisitive minds applied the OCTA prototypes to understanding diseases such as macular degeneration, diabetic retinopathy, and glaucoma. The technology's high resolution and ability to segment the different vascular layers provided novel insight into disease pathogenesis and morphology, providing a unique opportunity to investigate the ocular microvasculature in a level of anatomic detail that is not achievable with any other imaging strategy.

However, as with any new technology, OCTA has limitations that should be taken into account when interpreting its results, in both the research and clinical settings. Image artifacts and the inability to accurately quantify vascular parameters are some of the broadly recognized limitations, in addition to others related to variable segmentation algorithms and to the physics of image acquisition and processing. Today, advancements in software that address some of the limitations and more widespread access to the OCTA devices allow investigators to further expand upon our collective knowledge of ophthalmologic disease. In this special issue, we compiled a collection of high-quality research articles to discuss the state-of-the-art application of OCTA to chorioretinal diseases.

Five papers are included in this special edition that focus on a variety of different diseases and innovative applications of OCTA. One of these papers is a review of the choriocapillaris changes seen in advanced age-related macular degeneration (AMD) noting that OCTA has contributed significantly to our knowledge of the development and progression of geographic atrophy and choroidal neovascularization (CNV). The manuscript highlights that choriocapillaris atrophy occurs underneath and beyond the region of photoreceptor and retinal pigment epithelium loss and that CNV seems to originate from these areas of choriocapillaris alterations. A second paper included in this special edition also utilizes OCTA to study AMD but focuses on its value at the outer retina. The paper explores the changes seen in CNV after anti-vascular endothelial growth factor in treatment-naïve eyes compared with previously treated eyes. Qualitatively, the two groups respond similarly to treatment, but, quantitatively, the treatment-naïve eyes demonstrate a statistically significant decrease in CNV size while there is no difference in CNV size in the eyes that were previously treated.

A third paper focuses on the use of OCTA in detecting silent type 1 CNV in patients with chronic central serous chorioretinopathy. The authors show that OCTA delineates CNV in 8.3% of the treatment-naïve eyes in which OCT and fluorescein angiography (FA) did not show a CNV. A fourth paper compares the sensitivity and specificity of detection of polypoidal choroidal vasculopathy (PCV) using OCT and FA together with the sensitivity and specificity of OCT,

FA, and OCTA together. The work demonstrates that specificity is not improved when adding OCTA to the arsenal but sensitivity of PCV detection is enhanced from 69.5% to 90%. Lastly, the fifth paper employs the flow density function of OCTA to prospectively compare macular and optic nerve head vascular flow before and after cataract surgery plus implantation of two iStents and before and after cataract surgery alone. The authors demonstrate that there is statistically improved flow density in the macula and optic nerve head after cataract surgery plus iStent implantation but no change in eyes that underwent cataract surgery alone. These five manuscripts demonstrate interesting new applications of OCTA, contributing even further to both our understanding of the new technology and to the chorioretinal vascular diseases that are under investigation. As the scientific community moves forward with additional technological advances on OCTA, clinicians come together to establish new treatment paradigms based on this revolutionary imaging modality.

Talisa E. de Carlo
Nadia K. Waheed
Jayanth Sridhar
Daniela Ferrara

Hindawi
Journal of Ophthalmology
Volume 2018, Article ID 3751702, 7 pages
https://doi.org/10.1155/2018/3751702

Research Article

Optical Coherence Tomography Angiography to Distinguish Changes of Choroidal Neovascularization after Anti-VEGF Therapy: Monthly Loading Dose versus Pro Re Nata Regimen

Alexandra Miere,[1] Hassiba Oubraham,[1] Francesca Amoroso,[1] Pauline Butori,[1] Polina Astroz,[1] Oudy Semoun,[1] Elsa Bruyere,[1] Alexandre Pedinielli,[1] Manar Addou-Regnard,[1] Camille Jung,[2] Salomon Y. Cohen,[1,2] and Eric H. Souied[1,2]

[1]*Department of Ophthalmology, University Paris Est Créteil, Centre Hospitalier Intercommunal de Créteil, Créteil, France*
[2]*Clinical Research Center and Biological Resources Center, GRC Macula, Centre Hospitalier Intercommunal de Créteil, Créteil, France*

Correspondence should be addressed to Eric H. Souied; esouied@hotmail.com

Received 4 October 2017; Accepted 10 December 2017; Published 4 February 2018

Academic Editor: Talisa E. de Carlo

Purpose. To compare the qualitative and quantitative choroidal neovascularization (CNV) changes after antivascular endothelial growth factor (anti-VEGF) therapy in treatment-naïve and treated eyes with age-related macular degeneration (AMD) using optical coherence tomography angiography (OCTA). *Methods.* Consecutive patients with neovascular AMD underwent multimodal imaging, including OCTA (AngioPlex, CIRRUS HD-OCT model 5000; Carl Zeiss Meditec, Inc., Dublin, OH) at baseline and at three monthly follow-up visits. Treatment-naive AMD patients undergoing anti-VEGF loading phase were included in group A, while treated patients were included in group B. Qualitative and quantitative OCTA analyses were performed on outer retina to choriocapillaris (ORCC) slab. CNV size was measured using a free image analysis software (ImageJ, open-source imaging processing software, 2.0.0). *Results.* Twenty-five eyes of 25 patients were enrolled in our study (mean age 78.32 ± 6.8 years): 13 treatment-naïve eyes in group A and 12 treated eyes in group B. While qualitative analysis revealed no significant differences from baseline to follow-up in the two groups, quantitative analysis showed in group A a significant decrease in lesion area ($P = 0.023$); in group B, no significant change in the lesion area was observed during anti-VEGF therapy ($P = 0.93$). *Conclusion.* Treatment-naïve and treated eyes with CNV secondary to neovascular AMD respond differently to anti-VEGF therapy. This should be taken into account when using OCTA for CNV follow-up or planning therapeutic strategies.

1. Introduction

Paradigms concerning age-related macular degeneration have been shifting rapidly over the last decade, due to both therapeutic advances (i.e., antivascular endothelial growth factor therapy for neovascular AMD) and retinal imaging advances; among which, spectral domain optical coherence tomography, enhanced depth imaging optical coherence tomography, and optical coherence tomography angiography are noteworthy. OCTA is a new retinal imaging technique providing information on the actual location of the choroidal neovascularization, on various abnormalities of the retinal and choroidal microvasculature in a noninvasive manner [1–3]. Its exponential growth over the last few years asserts for its usefulness not only in an academic setting (giving insights into the pathogenesis of several macular disease), but also in a clinical setting [4–6].

Nevertheless, SD-OCT is a key element in detecting recurrences, and treatment decisions are frequently based solely on this noninvasive imaging method [7–9]. Classically,

recurrences of CNV are defined on SD-OCT by a myriad of signs, ranging from subretinal or intraretinal fluid, subretinal hyperreflective material, or changes in the pigment epithelial detachment's height [7–11]. When comparing these signs to fluorescein angiography (where the presence of late leakage or dye pooling is the central element in defining the presence of CNV) [12, 13] or indocyanine green angiography (which allows a clear visualization in its late frames of occult CNV) [14], the consequent conclusion is that of a growing complexity and greater refinement of the diagnosis provided by retinal imagery over time. However, while the signs provided by SD-OCT or conventional angiography are used to define activity of CNV to this day in a clinical setting, the concept of CNV activity itself involves more complicated, intricate mechanisms than previously thought [15]. Moreover, recent fundamental research studies have concluded that, in addition to elevated VEGF levels, dysregulated inflammation and autoimmunity play an essential role in CNV pathogenesis [16, 17].

In parallel to the complexity of CNV seen as either/or a disease or a compensatory response [15, 18], the management of neovascular AMD has been revolutionized by a series of pharmaceutical agents, such as ranibizumab (Lucentis; Genentech Inc., South San Francisco, CA), [19] aflibercept (Eylea; Regeneron Inc., Tarrytown, NJ), [20], and the off-label option bevacizumab (Avastin; Genentech Inc.), [21] which all inhibit VEGF-A. Moreover, multiple management strategies have been employed for anti-VEGF therapy, such as monthly dosing, every other month dosing after 3 initial monthly loading phase [20], and monthly loading phase followed by pro re nata (PRN) retreatment on evidence of exudative disease activity [22], as well as treat and extend regimens [23].

In our study, we aimed to compare the OCTA characteristics (using both qualitative and quantitative criteria) of eyes with neovascular AMD undergoing the monthly loading phase (treatment-naïve at baseline) versus eyes undergoing an as needed (PRN) regimen (previously treated at baseline).

2. Methods

2.1. Study Population. All consecutive patients of at least 60 years, presenting at the Montargis Eye Clinic (France) and Department of Ophthalmology of University Paris Est, in Creteil, France, between August 2016 and January 2017, diagnosed with treatment-naive or treated neovascular AMD were enrolled in this prospective comparison of qualitative and quantitative features of CNV undergoing anti-VEGF therapy in the loading phase (treatment-naive patients) and pro re nata regimen (treated patients). Visual outcomes from baseline to final visit were also assessed.

Diagnosis of type 1 and type 2 CNV was based on fundus biomicroscopy, fluorescein angiography (FA), and SD-OCT (CIRRUS HD-OCT model 5000, Carl Zeiss Meditec Inc., Dublin, California, USA). Only eyes with baseline presence of subretinal hyperreflective material (SHRM), intraretinal or subretinal fluid (SRF), and pigment epithelial detachment (PED) were included.

Two distinct groups were emerged: treatment-naive AMD patients undergoing anti-VEGF loading phase were included in group A, while previously treated patients undergoing PRN were included in group B.

Exclusion criteria consisted in type 3 neovascularization, media opacities, evidence of diabetic retinopathy or any other macular or retinal vascular disease, signs or history of central serous chorioretinopathy, and hereditary retinal dystrophy. Patients with poor quality images in OCTA were also excluded from the analysis. The study was performed in agreement with the Declaration of Helsinki for research involving human subjects and the French legislation. Our local Institutional Review Board approval was obtained for this study.

2.2. Study Protocol. At baseline, each enrolled patient underwent a complete ophthalmic examination including best-corrected visual acuity (BCVA), slit-lamp examination, fundus biomicroscopy FA, SD-OCT, and OCTA. OCTA was performed through AngioPlex CIRRUS HD-OCT model 5000 (Carl Zeiss Meditec Inc., Dublin, California, USA). OCTA was performed in all patients using a scanning area of 3×3 mm, centered on the fovea.

AngioPlex uses optical microangiography, which is an imaging technique that produces tridimensional images of dynamic blood perfusion at an imaging depth up to 2.0 mm [24, 25]. The instrument has an A-scan rate of 68,000 scans per second, using a superluminescent diode centered on 840 nm. The resultant 3×3 angio cube contains 245 B-scan slices repeated up to 4 times at each B-scan position. Each B-scan is made up of 245 A-scans; each A-scan is 1024-pixel deep [26].

Each included patient underwent 3 monthly visits following inclusion. BCVA, SD-OCT, and OCTA were performed during these follow-up visits. For patients included in group A (treatment-naive), an intravitreal injection was performed after the follow-up visit, while for patients included in group B, treatment indication was based on the presence/absence of classical activity signs on SD-OCT.

Two independent masked readers performed a qualitative and quantitative assessments. Qualitative analysis of OCTA ORCC segmentation images at baseline and at each follow-up visit consisted in morphological criteria from recent literature, [3–6, 27–29] such as presence/absence of a high-flow network, presence/absence of tiny ramifications, presence/absence of feeder vessel, presence/absence of an anastomotic arcade, presence/absence of a dark halo, presence/absence of flow void, and presence/absence of arteriolized vessels. All images were analyzed by the two independent readers using the outer retina to choriocapillaris (ORCC) slab, which allows a good visualization of type 1 and type 2 CNV important features [30]. Quantitative analysis of CNV size was performed on the same slab, using free image analysis software (ImageJ, open-source imaging processing software, 2.0.0-rc-43/1,51 K).

Quantitative and qualitative changes on OCTA were then compared between the two groups and correlated with best-corrected visual acuity (BCVA) and exudation signs on structural spectral domain (SD-OCT).

2.3. Statistical Analysis. Statistical data analysis was carried out using the STATA software (version 13.0, STATACORP LP, College Station, TX, USA). Qualitative variables were described in percentages, and quantitative variables were described by mean with standard deviation or by median with interquartile range. Intragroup serial comparisons of categorical variables at baseline and month 3 were carried out using the Wilcoxon signed-rank test. Intragroup serial comparisons of continuous variables at baseline and follow-up were carried out using the Exact McNemar signification probability test. Intergroup serial comparisons were carried out using Mann–Whitney test for categorical variables and Pearson's chi-square for continuous variables. Cohen's kappa coefficient was used to measure the interuser agreement for qualitative items on OCTA at baseline and follow-up. The chosen level of statistical significance was $P < 0.05$.

3. Results

3.1. Demographic Information. Twenty-five eyes of twenty-five patients were enrolled in our study (13 females, 12 males, mean age 78.32 ± 6.8 years). The final cohort for analysis consisted of 2 groups:

(i) Group A: 13 treatment-naïve eyes of 13 patients (7 females, 6 males, mean age 80.3 ± 7.57 years) that underwent monthly loading phase.

(ii) Group B: 12 previously treated eyes (6 females, 6 males, mean age 76.16 ± 5.37) by a mean of 7.16 ± 2.94 anti-VEGF intravitreal injections. Mean time from the diagnosis was 13.1 ± 2.56 months.

BCVA for the cohort as a whole at baseline was 60.64 ± 16.88 letters (Snellen equivalent 20/64). Baseline BCVA for eyes included in group A was 57.54 ± 20.52 letters (Snellen equivalent 20/80), while in group B baseline BCVA averaged 64 ± 11.78 letters (Snellen equivalent 20/50). Mean follow-up for both groups was 3 months.

3.2. Qualitative Assessment: Morphological OCTA Changes in the Monthly Loading Phase (Group A) versus PRN Phase (Group B) Eyes. At each visit, a high flow network in the ORCC slab was visualized in all cases (25/25). There was no statistical significant change in either of the above-mentioned features (presence/absence of a high-flow network, ramifications, feeder vessel, anastomotic arcade, dark halo, feeder vessel, and arteriolized vessels) in groups A and B, respectively, from baseline to month 3 (P ranging from 0.08 to 1). Table 1 shows the detailed morphological assessment of OCTA ORCC segmentation images.

3.3. Quantitative Assessment: OCTA Lesion Area Changes in the Monthly Loading Phase (Group A) versus PRN Phase (Group B) Eyes. In the group undergoing monthly loading dose (group A), there was a statistically significant decrease in the lesion area, from $0.66 \pm 0.84\,mm^2$ at baseline to $0.23 \pm 0.3\,mm^2$ at month 3 ($P = 0.02$, Wilcoxon signed-rank test). However, in the previously treated group now undergoing PRN regimen (group B), the lesion area slightly increased, from $0.94 \pm 1.06\,mm^2$ at baseline to $0.98 \pm 1\,mm^2$ at month 3 ($P = 0.93$, Wilcoxon signed-rank test). Table 2, as well as Figures 1, 2, and 3, shows these changes.

Table 1: Comparison of categorical variables between baseline and month 3 in groups A (treatment-naive patients undergoing monthly loading phase) and B (treated patients undergoing PRN regimen). Note that there is no statistically significant morphological change between baseline and month 3 (computed P value) in either group.

	Categorical variables	M0	M1	M2	M3	Significance*
Group A $N = 13$	High-flow network	13	13	13	13	$P = 1$
	Ramifications	11	7	6	3	$P = 0.25$
	Feeder vessel	3	3	1	3	$P = 1$
	Anastomotic arcade	1	1	0	1	$P = 0.5$
	Dark halo	4	4	2	4	$P = 1$
	Flow void	1	1	1	1	$P = 0.5$
	Arteriolized vessels	1	1	2	3	$P = 0.8$
Group B $N = 12$	High-flow network	12	12	11	11	$P = 1$
	Ramifications	10	8	6	6	$P = 0.13$
	Feeder vessel	4	4	4	4	$P = 1$
	Anastomotic arcade	4	2	2	2	$P = 1$
	Dark halo	8	9	8	5	$P = 0.25$
	Flow void	2	1	0	3	$P = 0.5$
	Arteriolized vessels	3	4	4	6	$P = 0.25$

*Exact McNemar significance probability; P value computed between baseline and month 3.

3.4. Best-Corrected Visual Acuity Changes in the Monthly Loading Phase (Group A) versus PRN Phase (Group B) Eyes. At baseline, there was no statistically significant difference in terms of BCVA between the two groups ($P = 0.44$, Mann–Whitney test). However, during follow-up, there was a statistically significant improvement in group A from 57.54 ± 20.52 letters at baseline to 65.33 ± 22.33 letters at month 3 ($P = 0.009$, Wilcoxon signed-rank test). Conversely, in group B, there was no statistically significant change in BCVA, which averaged 64 ± 11.78 letters at baseline and 61.25 ± 26.36 letters at month 3 ($P = 0.4$, Wilcoxon signed-rank test).

3.5. Reproducibility for Qualitative and Quantitative Analyses. For the criteria used in the qualitative analysis of OCTA images, interuser agreement was 94.9% (Cohen's K coefficient 0.91, standard error 0.14). For the quantitative criteria, interclass correlation coefficient (ICC) was high for the lesion area measurement, averaging 0.97 (CI 95% 0.96–0.98).

4. Discussion

In our study, we showed the difference in terms of qualitative and quantitative features on OCTA between a group of treatment-naïve patients undergoing monthly loading phase and a group of previously treated patients undergoing PRN

Table 2: Comparison of continuous variables between baseline and month 3 in groups A and B. Note that the CNV area decreased significantly in group A ($P = 0.02$) from baseline to month 3 and that BCVA improved in a statistically significant manner in group A from baseline to month 3 ($P = 0.009$).

	Continuous variables	Baseline	Month 1	Month 2	Month 3	Significance*
Group A $N = 13$	CNV area (mm^2)	0.66 ± 0.84	0.49 ± 0.65	0.28 ± 0.42	0.23 ± 0.3	$P = 0.02$
	BCVA (letters)	57.54 ± 20.52	57.14 ± 24.58	58.07 ± 26.05	64.15 ± 22.32	$P = 0.009$
Group B $N = 12$	CNV area (mm^2)	0.94 ± 1.06	0.92 ± 0.99	0.96 ± 1.01	0.98 ± 1.00	$P = 0.93$
	BCVA (letters)	64 ± 11.78	64 ± 17.67	56 ± 25.25	62.66 ± 26.36	$P = 0.4$

*Wilcoxon signed-rank test, P value computed between baseline and month 3.

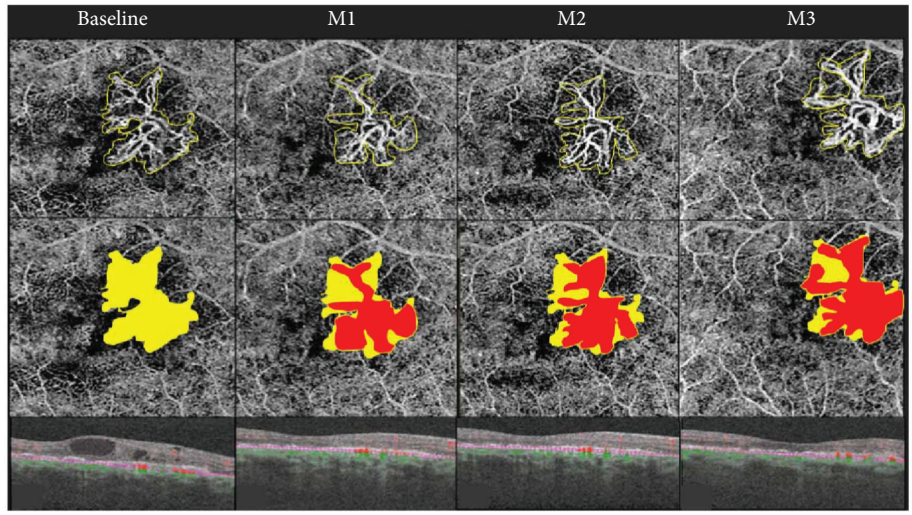

Figure 1: OCTA follow-up of treatment-naïve choroidal neovascularization (CNV) associated to neovascular age-related macular degeneration (AMD) during the monthly loading anti-VEGF phase. Each column represents a visit; the upper row represents the quantification of CNV size on the outer retina to choriocapillaris (ORCC) slab; the lower row represents the comparison between baseline lesion area (yellow) and follow-up CNV area (red). Quantitative analysis demonstrated that at baseline, the area in the ORCC segmentation averaged 1.06 mm^2. Under anti-VEGF therapy, this area decreased significantly, to 0.55 mm^2, at month 1 (M1). At month 2 (M2), the area averaged 0.72 mm^2, while at month 3 (M3), at the end of the loading phase, the CNV area was 0.87 mm^2. Indeed, the CNV area decreased from baseline to month 3 by 17.39%. This decrease has been noticed on the overall cohort of treatment-naïve in a statistically significant manner ($P = 0.02$, Figure 3).

regimen. While for the qualitative chosen criteria there was no statistically significant difference between the two groups, we note a higher prevalence of features associated with vascular immaturity (the presence of capillary sprouting, harboring the aspect of tiny ramifications within the neovascular membrane) [6, 29, 31] at baseline in the treatment-naïve group (group A) when compared to the treated group (group B). Conversely, in group B, the presence of arteriolized vessels, suggesting vascular maturity, [29] was higher (5/12) at baseline and progressively increased during follow-up.

Concerning lesion size as measured on the ORCC segmentation on OCTA images in the two groups, there was a significant decrease of the neovascular membrane size from baseline to month 3 in group A, suggesting that lesion size can be considered as a marker of therapeutic response to anti-VEGF in treatment-naïve nAMD patients. However, in group B, which had been diagnosed with nAMD 13.1 ± 2.56 months earlier and thus treated by a mean of 7.16 ± 2.94 anti-VEGF intravitreal injections, the neovascular membrane's area slightly increased over time (from $0.94 \pm 1.06\,mm^2$ at baseline to $0.98 \pm 1\,mm^2$ at month 3), suggesting that, for treated patients with medium to longstanding diagnosis of nAMD, a lesion size might be a questionable marker in assessing therapeutic response. As for the best-corrected visual acuity, there was a significant improvement ($P = 0.009$) only in group A, while in group B, the visual acuity did not improve significantly ($P = 0.40$) over the 3 months of follow-up.

Follow-up of nAMD by means of OCTA has been emphasized in the last years in the recent literature. Lumbroso et al. described, in 2015, the morphological changes within the type 2 neovascular membrane in neovascular AMD undergoing anti-VEGF treatment, suggesting the presence of patterns of cyclic CNV variations during follow-up and stating that the CNV cycle is 62 days long. [31]. Furthermore, Coscas et al. estimated that different CNV patterns

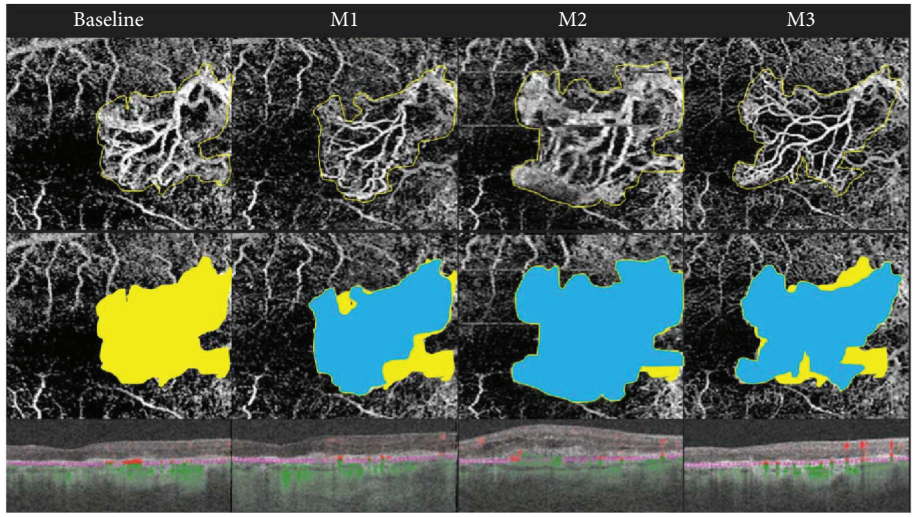

Figure 2: OCTA follow-up of previously treated choroidal neovascularization (CNV) associated to neovascular age-related macular degeneration (AMD) during pro re nata (as needed) regimen. Each column represents a visit; the upper row represents the quantification of CNV size on the outer retina to choriocapillaris (ORCC) slab; the lower row represents the comparison between the baseline lesion area (yellow) and follow-up CNV area (blue). Quantitative analysis demonstrated that at baseline, the area in the ORCC segmentation averaged 1.93 mm^2. Under anti-VEGF therapy, this area decreased to 1.85 mm^2, at month 1(M1). At month 2 (M2), the area increased to 2.92 mm^2, while at month 3 (M3), at the last follow-up visit, the CNV averaged 2.45 mm^2. Indeed, the CNV area slightly increased from baseline to month 3 by 26.94%. This expansion of the CNV size in treated patients has been noticed on the overall cohort ($P = 0.94$, Figure 3).

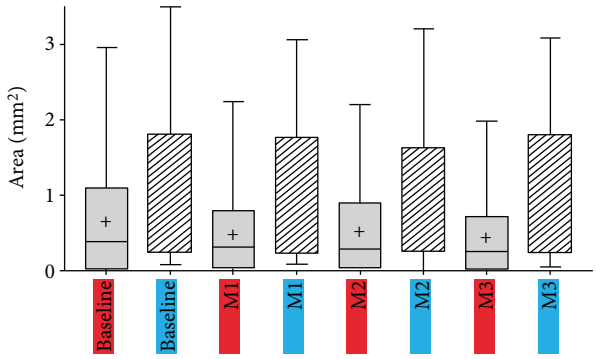

Figure 3: Box-and-whisker plot showing the comparison of CNV size between groups A and B. Group A (grey box on the plot; group A consists of treatment-naïve patients undergoing monthly loading phase) and group B (stripped box; group B consists of treated patients undergoing treatment according to a pro re nata regimen). Note that at baseline the treatment-naïve patients (grey box) had a smaller lesion size than the patients that had already been treated by anti-VEGF (stripped box). During the loading phase, treatment-naïve patients showed a statistically significant decrease in CNV size ($P = 0.02$), while the treated patients undergoing PRN regimen demonstrated a slight increase in the lesion size ($P = 0.93$) at month 3.

detected on OCTA had a correspondence with treatment decisions by multimodal imaging on their cohort [32]. Moreover, Muakkassa et al. approached this characterization of treatment-naïve CNV after anti-VEGF treatment on a larger spectrum of retinal pathology (from naMD to neovascularized idiopathic macular telangiectasia or multifocal choroiditis), also measuring the greatest linear dimension and area of these CNV. Their results showed that both of these categorical variables decreased (by 23.6% for greatest linear dimension and 29.8% for area, resp.) after anti-VEGF treatment [4]. Huang et al. revealed that the quantitative measurements of CNV flow area revealed a shutdown of flow 2 weeks after the injection, with reappearance of the CNV vascular channels in week four and actual exudative signs in week 6 [33].

On one hand, OCTA follow-up of CNV mentioned above strongly suggested the existence of a lifecycle of the CNV, with area being one of the markers for treatment response [6]. Spaide et al. made significant observations on the evolution of treated eyes with advanced nAMD using OCTA, by focusing on two vascular phenomena, arteriogenesis and angiogenesis, in an attempt to explain the longstanding persistence and change in morphology (vessel arteriolization) in patients with longstanding nAMD [29].

Taking these observations into consideration altogether with the variation in lesion area in our two groups, there may actually be two different responses to anti-VEGF therapy depending on disease duration (and thus of CNV immaturity/maturity). We hypothesize that in immature, treatment-naïve CNV there will be an initial response to treatment, characterized by regression (contraction) of the lesion area; this initial response to anti-VEGF shall be replaced in time by a late response, in which despite the disappearance of exudative signs of CNV, their area will continue to expand. The latter type of response corresponds to a mature CNV. The two types of response are illustrated in Figure 4.

Our study has several limitations, among which the most important are the small sample size and the heterogeneity of

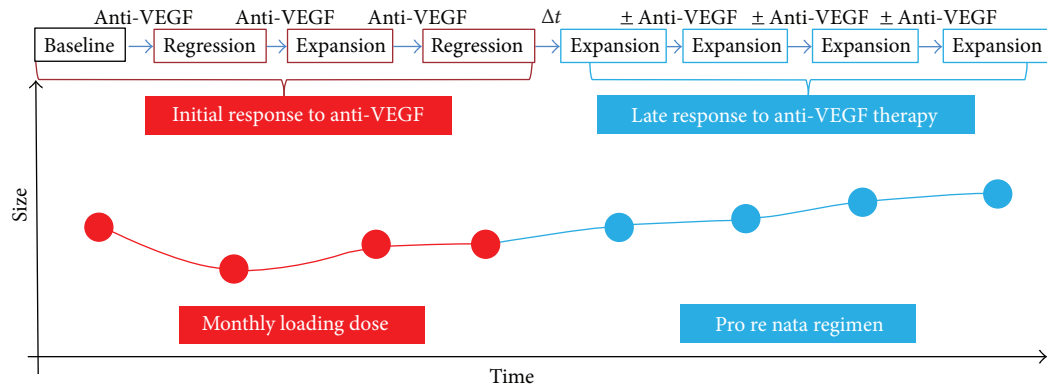

Figure 4: Illustrative drawing of suggested types of response to antiangiogenic treatment in CNV associated to neovascular AMD. Treatment-naïve, immature CNV, undergoing monthly loading phase, is depicted in red. Previously treated CNV, undergoing PRN, is depicted in blue. In the treatment-naïve eyes, there will be an initial response to treatment, characterized by regression (contraction) of the lesion area after each intravitreal injection (red dots). This initial response to anti-VEGF may be replaced after a variable amount of time(Δt) in an as needed protocol (PRN) by a late response in which, despite the disappearance of exudative signs of CNV, their area will continue to expand (blue dots). The latter type of response corresponds to a mature CNV.

our cohort. Last but not least, artifacts are still an important issue in OCTA technology. The slab we used to analyze OCTA images, given the hyperreflectivity of the retinal pigment epithelium (RPE), includes projection artifacts from the overlying superficial capillary plexus. Thus, we have analyzed images with and without projection artifact in order to correctly delineate the neovascular membrane.

In conclusion, our results suggest that there are two types of treatment responses to anti-VEGF, depending upon disease duration. Our data has two main corollaries: firstly, on the validity of a PRN treatment regimen, leaving therapeutic windows that could favor the growth and possibly the maturation of CNV. Secondly, on the way we should assess treatment response by OCTA in a clinical setting, taking into account disease duration and previous treatment. Of course, prospective studies on larger cohorts with a long follow-up should be performed in order to validate our findings.

Disclosure

Oudy Semoun is a consultant for Novartis (Basel, Switzerland), Bayer Schering Pharma (Berlin, Germany), Allergan Inc. (Irvine, California, USA), and Optovue (Freemont, California, USA). Salomon Y. Cohen is a consultant for Alcon (Hünenberg, Switzerland), Allergan Inc. (Irvine, California, USA), Novartis (Basel, Switzerland), Bayer Schering Pharma (Berlin, Germany), Farmila-Thea (Clermont-Ferrand, France), and Roche (San Francisco, CA, USA). Eric H. Souied is a consultant for Novartis (Basel, Switzerland), Bayer Schering Pharma (Berlin, Germany), Allergan Inc. (Irvine, California, USA), and Farmila-Thea (Clermont-Ferrand, France).

Conflicts of Interest

The authors declare there is no conflict of interest regarding the publication of this paper.

References

[1] Y. Jia, O. Tan, J. Tokayer et al., "Split-spectrum amplitude-decorrelation angiography with optical coherence tomography," *Optics Express*, vol. 20, no. 4, pp. 4710–4725, 2012.

[2] L. Kuehlewein, T. C. Tepelus, L. An, M. K. Durbin, S. Srinivas, and S. R. Sadda, "Noninvasive visualization and analysis of the human parafoveal capillary network using swept source OCT optical microangiography," *Investigative Ophthalmology & Visual Science*, vol. 56, no. 6, pp. 3984–3988, 2015.

[3] L. Kuehlewein, M. Bansal, T. L. Lenis et al., "Optical coherence tomography angiography of type 1 neovascularization in age-related macular degeneration," *American Journal of Ophthalmology*, vol. 160, no. 4, pp. 739–748.e2, 2015.

[4] N. W. Muakkassa, A. T. Chin, T. de Carlo et al., "Characterizing the effect of anti-vascular endothelial growth factor therapy on treatment-naive choroidal neovascularization using optical coherence tomography angiography," *Retina*, vol. 35, no. 11, pp. 2252–2259, 2015.

[5] E. A. Novais, M. Adhi, E. M. Moult et al., "Choroidal neovascularization analyzed on ultra-high speed swept source optical coherence tomography angiography compared to spectral domain optical coherence tomography angiography," *American Journal of Ophthalmology*, vol. 164, pp. 80–88, 2016.

[6] E. Moult, W. Choi, N. K. Waheed et al., "Ultrahigh-speed sweptsource OCT angiography in exudative AMD," *Ophthalmic Surgery, Lasers and Imaging Retina*, vol. 45, no. 6, pp. 496–505, 2014.

[7] A. E. Fung, G. A. Lalwani, P. J. Rosenfeld et al., "An optical coherence tomography-guided, variable dosing regimen with intravitreal ranibizumab (Lucentis) for neovascular age-related macular degeneration," *American Journal of Ophthalmology*, vol. 143, no. 4, pp. 566–583.e2, 2007.

[8] Comparison of Age-related Macular Degeneration Treatments Trials (CATT) Research Group, M. G. Maguire, D. F. Martin et al., "Five-year outcomes with anti-vascular endothelial growth factor treatment of neovascular age-related macular degeneration: the comparison of age-related macular degeneration treatments trials," *Ophthalmology*, vol. 123, no. 8, pp. 1751–1761, 2016.

[9] A. Au, V. S. Parikh, R. P. Singh et al., "Comparison of anti-VEGF therapies on fibrovascular pigment epithelial detachments in age-related macular degeneration," *The British Journal of Ophthalmology*, vol. 101, no. 7, pp. 970–975, 2017.

[10] V. P. Shah, S. A. Shah, S. Mrejen, and K. B. Freund, "Subretinal hyperreflective exudation associated with neovascular age-related macular degeneration," *Retina*, vol. 34, no. 7, pp. 1281–1288, 2014.

[11] R. Ores, N. Puche, G. Querques et al., "Gray hyper-reflective subretinal exudative lesions in exudative age-related macular degeneration," *American Journal of Ophthalmology*, vol. 158, no. 2, pp. 354–361, 2014.

[12] C. V. Regatieri, L. Branchini, and J. S. Duker, "The role of spectral-domain OCT in the diagnosis and management of neovascular age-related macular degeneration," *Ophthalmic Surgery, Lasers & Imaging*, vol. 42, no. 4, pp. S56–S66, 2011.

[13] Macular Photocoagulation Study Group, "Occult choroidal neovascularization," *Archives of Ophthalmology*, vol. 114, p. 400, 1996.

[14] L. A. Yannuzzi, J. S. Slakter, J. A. Sorenson, D. R. Guyer, and D. A. Orlock, "Digital indocyanine green videoangiography and choroidal neovascularization," *Retina*, vol. 12, no. 3, pp. 191–223, 1992.

[15] R. F. Spaide, "Choroidal neovascularization," *Retina*, vol. 37, no. 4, pp. 609-610, 2017.

[16] Y. Wang, V. M. Wang, and C. C. Chan, "The role of anti-inflammatory agents in age-related macular degeneration (AMD) treatment," *Eye*, vol. 25, no. 2, pp. 127–139, 2011.

[17] K. Morohoshi, A. M. Goodwin, M. Ohbayashi, and S. J. Ono, "Autoimmunity in retinal degeneration: autoimmune retinopathy and age-related macular degeneration," *Journal of Autoimmunity*, vol. 33, no. 3-4, pp. 247–254, 2009.

[18] H. E. Grossniklaus and W. R. Green, "Choroidal neovascularization," *American Journal of Ophthalmology*, vol. 137, no. 3, pp. 496–503, 2004.

[19] D. M. Brown, P. K. Kaiser, M. Michels et al., "Ranibizumab versus verteporfin for neovascular age-related macular degeneration," *The New England Journal of Medicine*, vol. 355, no. 14, pp. 1432–1444, 2006.

[20] J. S. Heier, D. M. Brown, V. Chong et al., "Intravitreal aflibercept (VEGF trap-eye) in wet age-related macular degeneration," *Ophthalmology*, vol. 119, no. 12, pp. 2537–2548, 2012.

[21] Comparison of Age-related Macular Degeneration Treatments Trials (CATT) Research Group, D. F. Martin, M. G. Maguire et al., "Ranibizumab and bevacizumab for treatment of neovascular age-related macular degeneration: two-year results," *Ophthalmology*, vol. 119, no. 7, pp. 1388–1398, 2012.

[22] B. G. Busbee, A. C. Ho, D. M. Brown et al., "Twelve-month efficacy and safety of 0.5 mg or 2.0 mg ranibizumab in patients with subfoveal neovascular age-related macular degeneration," *Ophthalmology*, vol. 120, no. 5, pp. 1046–1056, 2013.

[23] J. J. Arnold, A. Campain, D. Barthelmes et al., "Two-year outcomes of "treat and extend" intravitreal therapy for neovascular age-related macular degeneration," *Ophthalmology*, vol. 122, no. 6, pp. 1212–1219, 2015.

[24] R. K. Wang, "Optical microangiography: a label free 3D imaging technology to visualize and quantify blood circulations within tissue beds in vivo," *IEEE Journal of Selected Topics in Quantum Electronics*, vol. 16, no. 3, pp. 545–554, 2010.

[25] L. An and R. K. Wang, "In vivo volumetric imaging of vascular perfusion within human retina and choroids with optical micro-angiography," *Optics Express*, vol. 16, no. 15, pp. 11438–11452, 2008.

[26] A. Carnevali, M. V. Cicinelli, V. Capuano et al., "Optical coherence tomography angiography: a useful tool for diagnosis of treatment-naïve quiescent choroidal neovascularization," *American Journal of Ophthalmology*, vol. 169, pp. 189–198, 2016.

[27] A. El Ameen, S. Y. Cohen, O. Semoun et al., "Type 2 neovascularization secondary to age-related macular degeneration imaged by optical coherence tomography angiography," *Retina*, vol. 35, no. 11, pp. 2212–2218, 2015.

[28] A. Miere, O. Semoun, S. Y. Cohen et al., "Optical coherence tomography angiography features of subretinal fibrosis in age-related macular degeneration," *Retina*, vol. 35, no. 11, pp. 2275–2284, 2015.

[29] R. F. Spaide, "Optical coherence tomography angiography signs of vascular abnormalization with antiangiogenic therapy for choroidal neovascularization," *American Journal of Ophthalmology*, vol. 160, no. 1, pp. 6–16, 2015.

[30] L. Roisman, Q. Zhang, R. K. Wang et al., "Optical coherence tomography angiography of asymptomatic neovascularization in intermediate age-related macular degeneration," *Ophthalmology*, vol. 123, no. 6, pp. 1309–1319, 2016.

[31] B. Lumbroso, M. Rispoli, and M. C. Savastano, "Longitudinal optical coherence tomography-angiography study of type 2 naive choroidal neovascularization early response after treatment," *Retina*, vol. 35, no. 11, pp. 2242–2251, 2015.

[32] G. Coscas, M. Lupidi, F. Coscas, C. Français, C. Cagini, and E. H. Souied, "Optical coherence tomography angiography during follow up: qualitative and quantitative analysis of mixed type I and II choroidal neovascularization after vascular endothelial growth factor trap therapy," *Ophthalmic Research*, vol. 54, no. 2, pp. 57–63, 2015.

[33] D. Huang, Y. Jia, M. Rispoli, O. Tan, and B. Lumbroso, "Optical coherence tomography angiography of time course of choroidal neovascularization in response to anti-angiogenic treatment," *Retina*, vol. 35, no. 11, pp. 2260–2264, 2015.

Hindawi
Journal of Ophthalmology
Volume 2018, Article ID 2890357, 5 pages
https://doi.org/10.1155/2018/2890357

Clinical Study

Changes in Flow Density Measured Using Optical Coherence Tomography Angiography after iStent Insertion in Combination with Phacoemulsification in Patients with Open-Angle Glaucoma

Maged Alnawaiseh, Viktoria Müller, Larissa Lahme, Ralph Laurent Merté, and Nicole Eter

Department of Ophthalmology, University of Muenster Medical Center, Muenster, Germany

Correspondence should be addressed to Maged Alnawaiseh; magedbonn@hotmail.de

Received 5 October 2017; Accepted 17 December 2017; Published 31 January 2018

Academic Editor: Talisa E. de Carlo

Purpose. To evaluate changes in flow density after the implantation of a trabecular microbypass stent (iStent) in combination with cataract surgery. *Methods*. A total of 48 eyes of 48 patients, who underwent either cataract surgery alone (cataract group) or cataract surgery with implantation of two iStent inject devices (iStent group), were prospectively included in this study. Intraocular pressure (IOP) and flow density data before and after surgery were extracted and analyzed. *Results*. In the iStent group, the mean IOP was 18.2 ± 3.3 mmHg prior to surgery and 13.2 ± 2.3 at follow-up, and this difference was statistically significant ($p < 0.001$). The mean IOP in the cataract group also improved significantly after surgery (before: 17.1 ± 2.4; after: 15.1 ± 2.7 $p = 0.003$). The flow density (whole en face) in the superficial and deep retinal OCT angiogram of the macula (superficial: $p = 0.002$; deep: $p = 0.034$) and in the ONH ($p = 0.011$) improved significantly after surgery in the iStent group. The differences in the cataract group were not significant. *Conclusions*. Flow density of the macula and ONH, as measured by OCTA, improved significantly after cataract surgery with iStent. Noninvasive quantitative analyses of flow density provide a new parameter, which can help for the monitoring of therapy success after glaucoma surgery.

1. Introduction

Glaucoma is a leading cause of irreversible blindness worldwide, and its prevalence is projected to rise in the future. The treatment of glaucoma is based on a lowering of intraocular pressure to minimize the risk of visual loss [1, 2].

Microinvasive glaucoma surgery (MIGS) has attracted increasing interest in recent years. The microbypass stent or iStent is a small intraocular implant, which is inserted ab interno, sits within Schlemm canal, and reduces the IOP in mild to moderate glaucoma combined with a favorable safety profile [3–6]. iStent implantation is often performed concurrently with phacoemulsification, and the combined operation has been shown to significantly outperform phacoemulsification alone in the lowering of IOP [4] and to be similar to cataract surgery in terms of associated complications [5].

Optical coherence tomography angiography (OCTA) is a new imaging technique, which enables visualization of blood flow in the retina and optic nerve head without intravenously injected dye and has been described in healthy subjects in various retinal diseases and in animal models [7–12]. It is also possible to quantify the blood flow in the retina and ONH using OCTA, and a number of studies have demonstrated a reduced disc perfusion in patients suffering from glaucoma with this imaging procedure [9, 13, 14].

The aim of this study is to evaluate the impact of iStent insertion in combination with phacoemulsification on the flow density of the macula and ONH as measured using OCTA.

2. Materials and Methods

2.1. Subjects and Selection Criteria. Twenty-four consecutive patients diagnosed with cataract and open-angle glaucoma whose IOP was uncontrolled using their antiglaucoma medication were prospectively included in this study. The study followed the tenets of the Declaration of Helsinki and was approved by the Ethics Committee of the University of Muenster, North Rhine Westphalia, Germany. A control group of 24 eyes of 24 patients who underwent phacoemulsification cataract surgery without iStent implantation was also included.

Patients with glaucoma other than open-angle glaucoma, peripheral anterior synechiae, media opacities preventing a gonioscopic view of the angle or high-quality imaging, dense cataract, vitreoretinal disease, or neurological disease were excluded from the study.

Surgery was performed under topical or general anesthesia. In the cataract group, patients underwent a standard clear corneal phacoemulsification with implantation of a foldable IOL. In the iStent group, the standard clear corneal phacoemulsification was followed by an iStent implantation (Glaukos Corporation, Laguna Hills, CA). The surgical technique has been described in previous publications. In brief, after performing a standard clear corneal phacoemulsification with implantation of a foldable IOL, acetylcholine was injected into the anterior chamber to constrict the pupil. Next, the anterior chamber was filled with a viscoelastic agent (Healon, Abbott Medical Optics, Santa Ana, California, USA) to improve visualization of the angle and then, under gonioscopic view, two iStents were implanted through the trabecular meshwork into Schlemm's canal [5, 15].

2.2. Examination. All patients underwent a complete ocular examination including refraction, IOP measurement (Goldmann applanation tonometer), slit lamp biomicroscopy, gonioscopy, funduscopy, and OCT angiography imaging before and after surgery. OCT angiography imaging was obtained using the AngioVue OCTA system (RTVue XR Avanti with AngioVue, Optovue Inc, Fremont, California, USA). The system has an A-scan rate of 70,000 scans per second using a light source centered on 840 nm and a bandwidth of 45 nm. The split-spectrum amplitude-decorrelation angiography (SSADA) algorithm was used to extract the OCT angiography information. OCTA visualizes blood flow by means of technology described in detail in various studies in the literature. To visualize flow, OCT scans of a certain region are performed repeatedly and resultant OCT images are evaluated for changes. Whereas the blood flow in the retinal vessels will result in changes between subsequent OCT images, static tissue will show no change [8, 10, 16].

All OCTA imaging was performed under the same setting at the same location by an expert examiner and before imaging patients were asked to take a rest of about 5 minutes [17]. Macula imaging was performed using 3.0×3.0 mm scans while images over the optic nerve head were performed with 4.5×4.5 mm scans. The software automatically segmented the tissue into 4 layers, in the macula (superficial, deep, outer retina, and choriocapillaris) and in the ONH (optic nerve head, vitreous, radial peripapillary capillary (RPC), and choroid). The segmentations of all examinations were checked, and the flow density data of the optic nerve head and the macula were then extracted and analyzed. The flow density data were evaluated in the superficial retinal OCT angiogram of the macula, the deep retinal OCT angiogram of the macula, and the radial peripapillary capillary (RPC) layer of the optic nerve head (ONH). Images with lines or gaps arising from poor signal strength or motion artifacts were not included in the study.

2.3. Data Analysis and Statistics. Data management was performed using Microsoft Excel 2013. IBM SPSS® Statistics 22 for Windows (IBM Corporation, Somers, NY, USA) was used for statistical analyses. The normality of the data distribution was tested using the Kolmogorov-Smirnov test. After confirmation of the normality assumption, data are generally presented as mean ± standard deviation and changes at subsequent follow-up compared with baseline were assessed using paired sample t-tests. The two treatment groups were compared using independent Student's t-tests. The global statistical significance level was set to 0.05. All inferential statistics are intended to be exploratory, not confirmatory, and are interpreted accordingly.

3. Results

In this prospective study, 24 eyes of 24 patients with cataract and open-angle glaucoma (age 73.5 ± 6.2 years, 14 female, 10 male) were consecutively enrolled in the iStent group. Another 24 eyes of 24 patients (age 72.8 ± 8.9 years, 14 female, 10 male) were enrolled in the cataract group. There was no significant difference in age ($p = 0.770$) between the two groups.

In the iStent group, the mean IOP was 18.2 ± 3.3 mmHg prior to surgery and 13.2 ± 2.3 at follow-up, and this difference was statistically significant ($p < 0.001$). The IOP in the cataract group also improved significantly after surgery (before: 17.1 ± 2.4; after: 15.1 ± 2.7; $p = 0.003$). There was no statistically significant difference in either groups between the preoperative and postoperative signal strength index (SSI) (macula: iStent group: before: 62.8 ± 7.3; after: 63.4 ± 7.9; $p = 0.70$; cataract group: before: 59.4 ± 6.0; after: 61.4 ± 7.0; $p = 0.14$; ONH: iStent group: before: 57.7 ± 8.0; after: 58.3 ± 9.5; $p = 0.87$; cataract group: before: 56.3 ± 8.0; after: 60.9 ± 8.3; $p = 0.06$).

In the iStent group, the flow density (whole en face), as measured in the superficial and deep OCT angiogram of the macula and in the RPC of the ONH, improved significantly after surgery (superficial OCT angiogram: before: 44.6 ± 2.9; after: 47.6 ± 4.5; $p = 0.002$; deep OCT angiogram: before: 50.9 ± 3.6; after: 53.0 ± 4.2; $p = 0.034$; RPC: 43.5 ± 7.7; after: 45.4 ± 6.5). The flow density data of the iStent group are summarized in Table 1.

In the cataract group, there was no statistically significant difference between the preoperative and postoperative flow density whole en face (before surgery: 46.2 ± 2.5; after surgery: 47.1 ± 2.6; $p = 0.20$). The flow density data in the

Table 1: Characteristics of the study population in the iStent group and values of flow density obtained in the indicated regions before and after surgery. Bold: statistically significant differences.

(a)

iStent group	
N	24
Age (years)	73.46 ± 6.24
Gender (female : male)	14 : 10

(b)

	Before surgery mean ± SD	After surgery mean ± SD	*p* value
IOP	18.17 ± 3.25	13.21 ± 2.34	**<0.001**
OCTA—superficial			
Flow density (whole en face)	44.56 ± 2.89	47.61 ± 4.46	**0.002**
Flow density (fovea)	29.50 ± 5.42	31.99 ± 7.06	**0.016**
Flow density (parafovea)	46.62 ± 3.11	49.52 ± 4.53	**0.003**
OCTA—deep			
Flow density (whole en face)	50.86 ± 3.62	52.97 ± 4.22	**0.034**
Flow density (fovea)	29.21 ± 6.22	31.47 ± 8.24	0.063
Flow density (parafovea)	53.05 ± 4.37	54.89 ± 4.63	0.074
OCTA—RPC			
Flow density (whole en face)	43.53 ± 7.70	45.40 ± 6.54	**0.011**
Flow density (inside disc)	25.83 ± 12.50	28.58 ± 14.36	**0.012**
Flow density (peripapillary)	52.49 ± 8.32	53.17 ± 6.89	0.421

Table 2: Characteristics of the study population in the cataract group and values of flow density obtained in the indicated regions before and after surgery. Bold: statistically significant differences.

(a)

Cataract group	
N	24
Age (years)	72.79 ± 8.88
Gender (female : male)	14 : 10

(b)

	Before surgery mean ± SD	After surgery mean ± SD	*p* value
IOP	17.14 ± 2.36	15.10 ± 2.74	**0.003**
OCTA—superficial			
Flow density (whole en face)	46.22 ± 2.49	47.05 ± 2.59	0.200
Flow density (fovea)	28.18 ± 5.45	28.57 ± 4.87	0.740
Flow density (parafovea)	48.63 ± 2.56	49.07 ± 3.05	0.576
OCTA—deep			
Flow density (whole en face)	53.08 ± 2.42	54.20 ± 2.28	0.099
Flow density (fovea)	29.45 ± 6.78	31.15 ± 6.64	0.333
Flow density (parafovea)	55.99 ± 2.63	56.30 ± 3.62	0.668
OCTA—RPC			
Flow density (whole en face)	50.16 ± 4.81	50.04 ± 4.58	0.827
Flow density (inside disc)	39.95 ± 9.89	40.77 ± 9.39	0.294
Flow density (peripapillary)	58.73 ± 6.16	57.90 ± 5.73	0.228

cataract group before and after surgery are summarized in Table 2.

4. Discussion

The flow densities in the retinal OCT angiogram of the macula and in the radial peripapillary capillary (RPC) network, as measured using OCTA, improved significantly after iStent implantation in conjunction with cataract surgery.

The iStent has become an important player among microinvasive glaucoma surgeries. Compared with filtrating surgery, the procedure has a higher safety profile and shorter recovery time and is sparing of conjunctival tissue, should a more invasive procedure be necessary [5, 18]. Microinvasive glaucoma surgery (MIGS) is therefore becoming more popular. However, the reduction in intraocular pressure seen with the iStent is lower than that achievable with filtering surgery [5]. In clinical practice, this minimally invasive procedure is usually performed in combination with cataract extraction. This study demonstrates the "typical" clinical use of the device and explores the utility of OCTA in monitoring the success of a given treatment.

Optical coherence tomography (OCT) angiography is a new imaging technique, in which the retinal and choroidal circulation can be visualized without contrast agent. OCTA also enables a quantitative analysis of blood flow. The reproducibility and repeatability of flow density data as measured by OCT angiography have been evaluated in normal subjects and in glaucoma patients in different studies in the literature [13, 19, 20].

Evaluation studies on OCTA in patients suffering from glaucoma show a reduction of ONH and macula perfusion in glaucoma patients compared with healthy controls. The flow density data also correlate with disease severity as well as functional and structural damage [9, 21, 22]. Furthermore, Akil et al. demonstrated that vessel density measurements derived from noninvasive OCT angiography show a stepwise decrease from normal eyes to preperimetric glaucoma eyes to mild POAG eyes [22]. Holló demonstrated that OCT angiography is also able to detect transient changes in peripapillary perfusion noninvasively in glaucoma patients. In that study, the peripapillary flow density was evaluated in 6 eyes of 4 patients with IOP > =35 mmHg before and after topical treatment. In Holló's case series, the peripapillary flow density increased significantly after medical IOP reduction in all cases [23]. Our study evaluated the impact of iStent

combined with phacoemulsification in coexistent open-angle glaucoma and cataract on flow density measured using OCTA. To the best of our knowledge, this is the first study to evaluate the impact of a surgical lowering of IOP on flow density measurements. After cataract surgery in combination with iStent insertion, the vessel density (whole en face) improved significantly in the superficial retinal OCT angiogram of the macula, in the deep retinal OCT angiogram of the macula, and in the radial peripapillary capillary (RPC) layer of the optic nerve head (ONH). Although the IOP improved significantly after surgery in the cataract group, the differences of flow density were not significant. This may be explained by the relatively minor changes in IOP in the cataract group compared with the iStent group or by the small sample size.

This study is not without limitations. First, the image quality could be improved after cataract surgery, which might influence the flow density measurements. However, patients with media opacities preventing high-quality imaging and those with dense cataract were excluded from the study. In this context, it is also important to mention that there was no statistically significant difference between the pre- and postoperative signal strength index. Second, our study is also limited by its small sample size, and this should be considered when evaluating the outcome in the cataract group. However, this study was designed to evaluate the impact of iStent insertion in combination with phacoemulsification on flow density measurements and not to compare cataract surgery alone with cataract surgery in combination with iStent. This has been evaluated in other studies in the literature. Third, our results may have been affected by the short follow-up time. Further longitudinal studies involving larger numbers of patients are thus needed.

In conclusion, iStent insertion in combination with cataract extraction induced a significant improvement in macular and ONH perfusion. Not only does flow density, as measured by OCTA, appear to correlate with structural and functional glaucoma damage, but OCTA is also able to visualize acute changes in macula and ONH perfusion and can therefore be used to evaluate short-term therapy success.

Conflicts of Interest

The authors declare that there is no conflict of interest regarding the publication of this paper.

References

[1] Y. C. Tham, X. Li, T. Y. Wong, H. A. Quigley, T. Aung, and C. Y. Cheng, "Global prevalence of glaucoma and projections of glaucoma burden through 2040: a systematic review and meta-analysis," *Ophthalmology*, vol. 121, no. 11, pp. 2081–2090, 2014.

[2] H. A. Quigley and A. T. Broman, "The number of people with glaucoma worldwide in 2010 and 2020," *British Journal of Ophthalmology*, vol. 90, no. 3, pp. 262–267, 2006.

[3] M. S. Malvankar-Mehta, Y. N. Chen, Y. Iordanous, W. W. Wang, J. Costella, and C. M. L. Hutnik, "iStent as a solo procedure for glaucoma patients: a systematic review and meta-analysis," *PLoS One*, vol. 10, no. 5, article e0128146, 2015.

[4] M. S. Malvankar-Mehta, Y. Iordanous, Y. N. Chen et al., "iStent with phacoemulsification versus phacoemulsification alone for patients with glaucoma and cataract: a meta-analysis," *PLoS One*, vol. 10, no. 7, article e0131770, 2015.

[5] C. L. Larsen and T. W. Samuelson, "Managing coexistent cataract and glaucoma with iStent," *Survey of Ophthalmology*, vol. 62, no. 5, pp. 706–711, 2017.

[6] L. Voskanyan, J. García-Feijoó, J. I. Belda et al., "Prospective, unmasked evaluation of the iStent® *inject* system for open-angle glaucoma: synergy trial," *Advances in Therapy*, vol. 31, no. 2, pp. 189–201, 2014.

[7] M. Alnawaiseh, C. Brand, J. L. Lauermann, and N. Eter, "Flow density measurements using optical coherence tomography angiography: impact of age and gender," *Ophthalmologe*, 2017.

[8] Y. Jia, S. T. Bailey, D. J. Wilson et al., "Quantitative optical coherence tomography angiography of choroidal neovascularization in age-related macular degeneration," *Ophthalmology*, vol. 121, no. 7, pp. 1435–1444, 2014.

[9] P.-M. Lévêque, P. Zéboulon, E. Brasnu, C. Baudouin, and A. Labbé, "Optic disc vascularization in glaucoma: value of spectral-domain optical coherence tomography angiography," *Journal of Ophthalmology*, vol. 2016, Article ID 6956717, 9 pages, 2016.

[10] M. Quaranta-El Maftouhi, A. El Maftouhi, and C. M. Eandi, "Chronic central serous chorioretinopathy imaged by optical coherence tomographic angiography," *American Journal of Ophthalmology*, vol. 160, no. 3, pp. 581–587.e1, 2015.

[11] M. Alnawaiseh, F. Schubert, P. Nelis, G. Wirths, A. Rosentreter, and N. Eter, "Optical coherence tomography (OCT) angiography findings in retinal arterial macroaneurysms," *BMC Ophthalmology*, vol. 16, no. 1, p. 120, 2016.

[12] M. Alnawaiseh, A. Rosentreter, A. Hillmann et al., "OCT angiography in the mouse: a novel evaluation method for vascular pathologies of the mouse retina," *Experimental Eye Research*, vol. 145, pp. 417–423, 2016.

[13] G. Holló, "Intrasession and between-visit variability of sector peripapillary angioflow vessel density values measured with the angiovue optical coherence tomograph in different retinal layers in ocular hypertension and glaucoma," *PLoS One*, vol. 11, no. 8, article e0161631, 2016.

[14] X. Wang, C. Jiang, T. Ko et al., "Correlation between optic disc perfusion and glaucomatous severity in patients with open-angle glaucoma: an optical coherence tomography angiography study," *Graefe's Archive for Clinical and Experimental Ophthalmology*, vol. 253, no. 9, pp. 1557–1564, 2015.

[15] P. Arriola-Villalobos, J. M. Martínez-de-la-Casa, D. Díaz-Valle et al., "Mid-term evaluation of the new Glaukos iStent with phacoemulsification in coexistent open-angle glaucoma or ocular hypertension and cataract," *British Journal of Ophthalmology*, vol. 97, no. 10, pp. 1250–1255, 2013.

[16] R. F. Spaide, J. G. Fujimoto, and N. K. Waheed, "Image artifacts in optical coherence tomography angiography," *Retina*, vol. 35, no. 11, pp. 2163–2180, 2015.

[17] M. Alnawaiseh, L. Lahme, M. Treder, A. Rosentreter, and N. Eter, "Short-term effects of exercise on optic nerve and macular perfusion measured by optical coherence tomography angiography," *Retina*, vol. 37, no. 9, pp. 1642–1646, 2017.

[18] T. W. Samuelson, L. J. Katz, J. M. Wells, Y. J. Duh, J. E. Giamporcaro, and US iStent Study Group, "Randomized evaluation of the trabecular micro-bypass stent with

phacoemulsification in patients with glaucoma and cataract," *Ophthalmology*, vol. 118, no. 3, pp. 459–467, 2011.

[19] M. Al-Sheikh, T. C. Tepelus, T. Nazikyan, and S. V. R. Sadda, "Repeatability of automated vessel density measurements using optical coherence tomography angiography," *British Journal of Ophthalmology*, vol. 101, no. 4, pp. 449–452, 2017.

[20] F. Coscas, A. Sellam, A. Glacet-Bernard et al., "Normative data for vascular density in superficial and deep capillary plexuses of healthy adults assessed by optical coherence tomography angiography," *Investigative Ophthalmology & Visual Science*, vol. 57, no. 9, pp. OCT211–OCT223, 2016.

[21] H. S.-L. Chen, C.-H. Liu, W.-C. Wu, H.-J. Tseng, and Y.-S. Lee, "Optical coherence tomography angiography of the superficial microvasculature in the macular and peripapillary areas in glaucomatous and healthy eyes," *Investigative Ophthalmology & Visual Science*, vol. 58, no. 9, pp. 3637–3645, 2017.

[22] H. Akil, A. S. Huang, B. A. Francis, S. R. Sadda, and V. Chopra, "Retinal vessel density from optical coherence tomography angiography to differentiate early glaucoma, pre-perimetric glaucoma and normal eyes," *PLoS One*, vol. 12, no. 2, article e0170476, 2017.

[23] G. Holló, "Influence of large intraocular pressure reduction on peripapillary OCT vessel density in ocular hypertensive and glaucoma eyes," *Journal of Glaucoma*, vol. 26, no. 1, pp. e7–e10, 2017.

Hindawi
Journal of Ophthalmology
Volume 2018, Article ID 8125267, 6 pages
https://doi.org/10.1155/2018/8125267

Review Article

Choriocapillaris Loss in Advanced Age-Related Macular Degeneration

Carlos A. Moreira-Neto,[1,2] **Eric M. Moult**,[3] **James G. Fujimoto**,[3] **Nadia K. Waheed**,[1] **and Daniela Ferrara**[1]

[1]*Department of Ophthalmology, Tufts University School of Medicine, Boston, MA, USA*
[2]*Hospital de Olhos do Paraná, Curitiba, PR, Brazil*
[3]*Department of Electrical Engineering and Computer Science and Research Laboratory of Electronics, Massachusetts Institute of Technology, Cambridge, MA, USA*

Correspondence should be addressed to Daniela Ferrara; daniela@ferrara.md

Received 30 July 2017; Revised 29 November 2017; Accepted 11 December 2017; Published 30 January 2018

Academic Editor: Lisa Toto

The purpose of this review is to summarize the current knowledge on choriocapillaris loss in advanced age macular degeneration (AMD). Several histopathological studies in animal models and human eyes had showed that the choriocapillaris density decreases with age. However, the role of choriocapillaris loss is still unclear in AMD and its advanced forms, either choroidal neovascularization (CNV) or geographic atrophy (GA). Some authors have hypothesized that choriocapillaris loss might precede overt retinal pigment epithelium atrophy. Others have hypothesized that deposition of complement complexes on and around the choriocapillaris could be related to the tissue loss observed in early AMD. The development of imaging modalities, such as optical coherence tomography angiography (OCTA), have led to a better understanding of underlying physiopathological mechanisms in AMD. OCTA showed atrophy of choriocapillaris underneath and beyond the region of photoreceptors and RPE loss, in agreement with previous histopathologic studies. The evolution of OCTA technology suggests that CNV seems to originate from regions of severe choriocapillaris alteration. Significant progress has been made in the understanding of development and progression of GA and CNV. *In vivo* investigation of the choriocapillaris using OCTA may lead to new insights related to underlying disease mechanisms in AMD.

1. Introduction

A major biological function of the choriocapillaris is to supply oxygen and metabolites to the RPE and outer neurosensory retina, constituting the only route for metabolic exchange in the retina within the foveal avascular zone. This route is also responsible for removing and recycling the wastes from the neurosensory retina [1, 2].

Aging is a complex multifactorial process that leads to ultrastructural changes to the retinal pigment epithelium (RPE), Bruch's membrane, and choriocapillaris [3]. Electron microscopy has shown that aged human Bruch's membrane has abnormalities analogous to what was observed in descriptive and experimental studies of human systemic vascular aging and atherosclerosis [4]. Normal aging changes to the choriocapillaris have been described in experimental mouse models [5, 6] as well as human eyes [7], including ultrastructural damage to the endothelial cells and choriocapillaris atrophy [3]. Interestingly, the glomerulus of kidney is a comparison organ for the RPE-Bruch's membrane complex because of their common biological functions of filtration and molecular similarities of their basement membranes. Some of these aging changes in the eye are comparable to renal tubular epithelial cell changes associated with acute interstitial nephritis and acute tubular necrosis [3, 8, 9]. Ramrattan and colleagues showed in a morphometric study of 95 unpaired normal human aging eyes that the density of the choriocapillaris decreases with age [10]. Choriocapillaris endothelial cell fenestration loss was also observed adjacent to large outer collagenous layer deposits, but not with

isolated choriocapillaris basement membrane alterations, which may be a sign of cytotoxic injury in human aging eyes with age-related macular degeneration [11].

2. Choriocapillaris in GA

Advanced nonexudative age-related macular degeneration (AMD) is characterized by drusen, pigmentary changes, and eventual loss of photoreceptors, RPE, and choriocapillaris in a distinct geographic atrophy (GA) lesion. Although significant progress has been made in the understanding of risk factors associated with development and progression of AMD and GA, the role of choriocapillaris loss is still unclear. While RPE loss is the hallmark of GA lesions, some authors have recently hypothesized that photoreceptor loss or choriocapillaris loss might precede the overt RPE atrophy [12].

Extensive experimental and genetic evidences suggest a major role of the alternative complement pathway in the development of AMD and GA [13]. It has been hypothesized that deposition of complement pathway complexes on and around the choriocapillaris could be related to the choriocapillaris loss observed since early AMD, correlating with the abundance and size of drusen [14]. Mullins and colleagues investigated whether eyes from donors with a high-risk genotype associated with complement gene polymorphism exhibited altered levels of membrane attack complex (MAC) in the choroid, compared to eyes with a low-risk genotype. These authors showed that eyes from donors with high-risk genotype had 69% higher levels of MAC than low-risk controls, independent of any clinical signs of AMD. Their results provide evidence that high-risk complement-related genotypes may affect AMD risk by increased deposition of MAC around the aging choriocapillaris [15].

This same group evaluated the abundance of MAC in normal aging eyes, early AMD, and advanced AMD donor eyes. These authors found that samples from those with AMD had variable but significantly higher levels of MAC than either age-matched control eyes or younger eyes. Using MAC immunofluorescence, they found that in eyes with early AMD, small hard drusen were almost invariably labeled with anti-MAC antibody. In contrast to younger eyes and aged control eyes, extension of the MAC reactive domain often extended into the outer choroid. In the aging macula, MAC was predominantly localized to the outer aspect of Bruch's membrane and in extracellular domain surrounding the choriocapillaris. In eyes with GA, MAC was present in the choriocapillaris outside of areas of RPE and photoreceptor loss in a pattern similar to that seen in early AMD, although reactivity on outer vessel walls was more notable in eyes with GA. In areas of extensive atrophy, the intensity of immunoreactivity at the choriocapillaris/Bruch's membrane interface was lower than elsewhere, although a moderate level of anti-MAC labeling was found to persist even when RPE, photoreceptor, and choriocapillaris loss was complete [16].

Aiming at a better understanding of MAC accumulation in the choroid and other aging tissues, Chirco and colleagues studied the abundance of MAC across multiple human tissues. They concluded that selective accumulation of MAC in the choriocapillaris is a plausible explanation for the fact that individuals with high-risk genotypes develop AMD rather than an array of extraocular diseases. The choroid appears to be a "hot spot" for MAC deposition [17].

Zeng and colleagues describe the effects of complement exposure on choroidal endothelial cells in a system that models some aspects of AMD. Their results indicate that when choriocapillaris is exposed to MAC, choroidal endothelial cells are susceptible to complement-mediated cytolysis in a concentration- and dose-dependent manner [18].

Seddon and colleagues hypothesized, based on a histopathological study, that RPE atrophy might precede choriocapillaris loss in GA. However, they also observed that choriocapillaris loss occurred in the absence of RPE atrophy in few eyes with early AMD [19].

3. OCTA Documenting Choriocapillaris in GA

Optical coherence tomography (OCT) is a key imaging modality in the evaluation and management of chorioretinal diseases, allowing noninvasive optical reconstruction of the anatomy based on back-reflected light. Despite the ability of OCT to image *in vivo* structures with resolution approaching histological section, it is fundamentally limited in the detailed documentation of the microvasculature of the fundus [20].

To visualize chorioretinal vasculature without the need for intravenous dye, several OCT-based angiography technologies have been developed for a three-dimensional vascular mapping of the microcirculation [21]. OCT angiography (OCTA) is a new imaging modality that employs motion contrast imaging to high-resolution, dense volumetric datasets generating angiographic images noninvasively. OCTA computes the decorrelation signal, based on difference in the backscattered OCT signal intensity or amplitude between sequential OCT scans taken at precisely the same location, in order to generate a blood flow map [22]. OCTA requires higher imaging speeds than structural OCT because it acquires repeated B-scans at each retinal location. In addition, sophisticated algorithms are also required to manage image artifacts, ensuring that the resultant OCTA images represent strictly blood cells' movement in chorioretinal blood vessels [23, 24].

The dynamic range of OCTA is limited in commercially available devices, so there is a slowest detectable flow and a fastest distinguishable flow. Blood flowing below the slowest detectable flow produces decorrelation signals that cannot be separated from system noise and are therefore undetectable with the currently available technology. Blood flowing faster than the fastest distinguishable flow produces similar decorrelation and are therefore indistinguishable from one another [25].

Despite current limitations, OCTA provides a unique opportunity for *in vivo* assessment of the choriocapillaris. In patients with GA, OCTA with swept-source technology showed atrophy of choriocapillaris underneath the region of photoreceptor and RPE loss, in agreement with previous histopathologic studies [26, 27]. In some cases, choriocapillaris alterations on OCTA and histopathology related to impaired flow and dropout were found extending beyond

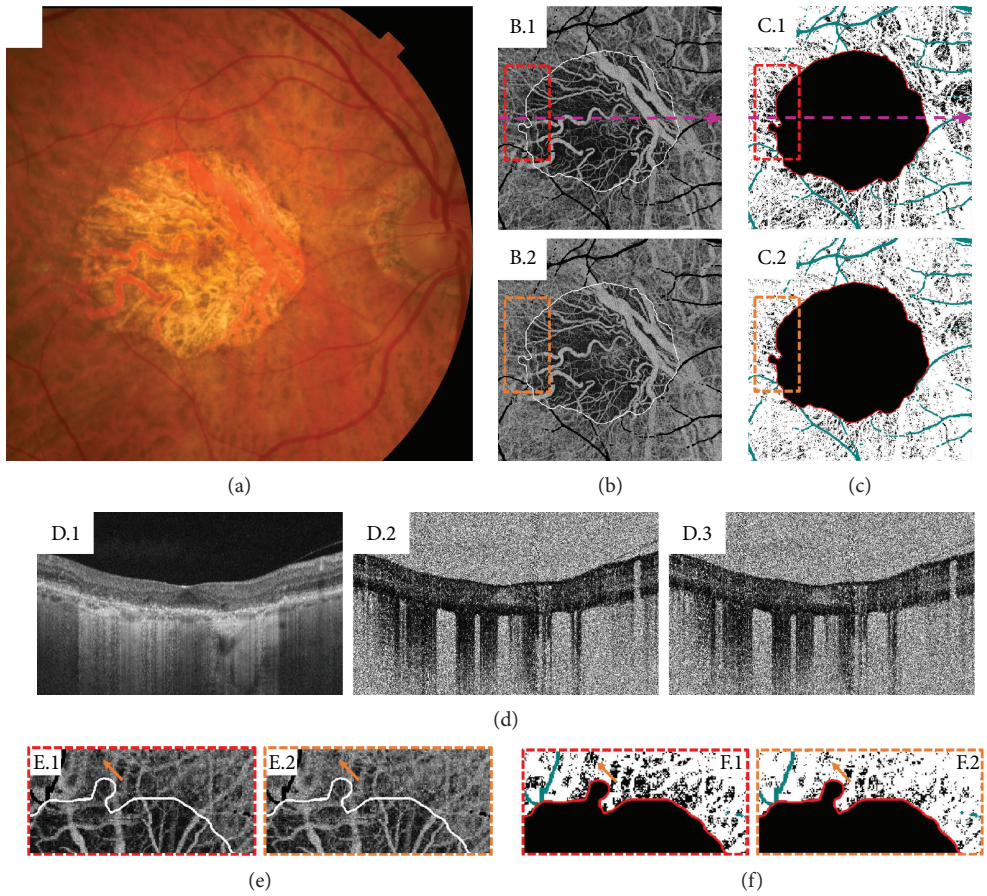

Figure 1: A 76-year-old patient with geographic atrophy (GA). (a) Color fundus photograph. (b) En face projections of a 6 mm × 6 mm, unthresholded optical coherence tomography (OCT) angiography (OCTA) volume from Bruch's membrane to 45 μm below. B.1 corresponds to a 1.5 ms interscan time OCTA volume, and B.2 corresponds to a 3.0 ms interscan time OCTA volume. Projection artifacts from large retinal vessels have been removed and colored black. The white contours trace the margin of atrophy, as determined by a subretinal pigment epithelium (RPE) slab of the OCT volume. Note that the 1.5 ms interscan OCTA image reveals substantially more choriocapillaris alteration than does the 3.0 ms interscan time image. In some regions, the OCTA signal is documented in the 3.0 ms interscan time but not the 1.5 ms interscan time, suggesting that these regions have flow impairment rather than complete choriocapillaris atrophy. (c) Binarized versions of the choriocapillaris OCTA images in B, where a constant threshold was used. C.1 corresponds to the 1.5 ms interscan time OCTA image, and C.2 corresponds to the 3.0 ms interscan time OCTA image. Again, note there are substantially more areas of low choriocapillaris flow (black) in the 1.5 ms interscan time OCTA image than in the 3.0 ms interscan time OCTA image. (d) OCT and OCTA B-scans extracted from the locations indicated by the dashed pink lines of B.1 and C.1. The OCT B-scan (D.1) shows RPE and photoreceptor loss, which causes increased light penetration into the choroid. The 1.5 ms OCTA B-scan is shown in D.2, and the 3.0 ms OCTA B-scan is shown in D.3. Note that both D.2 and D.3 are unthresholded OCTA images, which results in worse image quality. Unthresholded choriocapillaris OCTA images are useful for reducing the rate of false-positive flow impairment due to thresholding. (e-f) Enlargements of the dashed boxes in B-C. Red boxes correspond to 1.5 ms interscan time images, and orange boxes correspond to 3.0 ms interscan time images. The boxes have been rotated 90 degrees clockwise relative to their orientations in B and C. These regions of interest show that there is choriocapillaris flow impairment beyond the margin of RPE atrophy. Arrows point to an example area of flow impairment which changes as a function of interscan time. Note that in the 1.5 ms OCTA, there is less OCTA signal (more dark areas) than in the 3.0 ms OCTA, which makes the impairment more pronounced in the 1.5 ms OCTA (this is easiest seen in F.1 and F.2). This illustrates how shorter interscan time OCTA is more sensitive to flow alterations than is longer interscan time OCTA.

the margins of GA or between discrete areas of GA [16]. In other cases, however, choriocapillaris alterations on OCTA were grossly aligned with the boundaries of the GA lesion on fundus imaging [25].

Choi and colleagues used ultrahigh-speed swept-source OCTA and variable interscan time analysis (VISTA) algorithm to assess choriocapillaris changes in patients with GA. Although VISTA has the ability to shift the range downwards of the detectable flow speeds, these authors still highlighted some challenges in the interpretation of OCTA images. A low decorrelation signal may be observed due to a complete absence of flow and vasculature, secondary to true vascular atrophy. However, a low decorrelation signal may also be observed due to slow blood flow but intact vasculature, secondary to flow impairment only. Collectively, atrophy and flow impairment represent different types of choriocapillaris alteration. In this same study, OCTA with VISTA was used to study choriocapillaris flow alterations

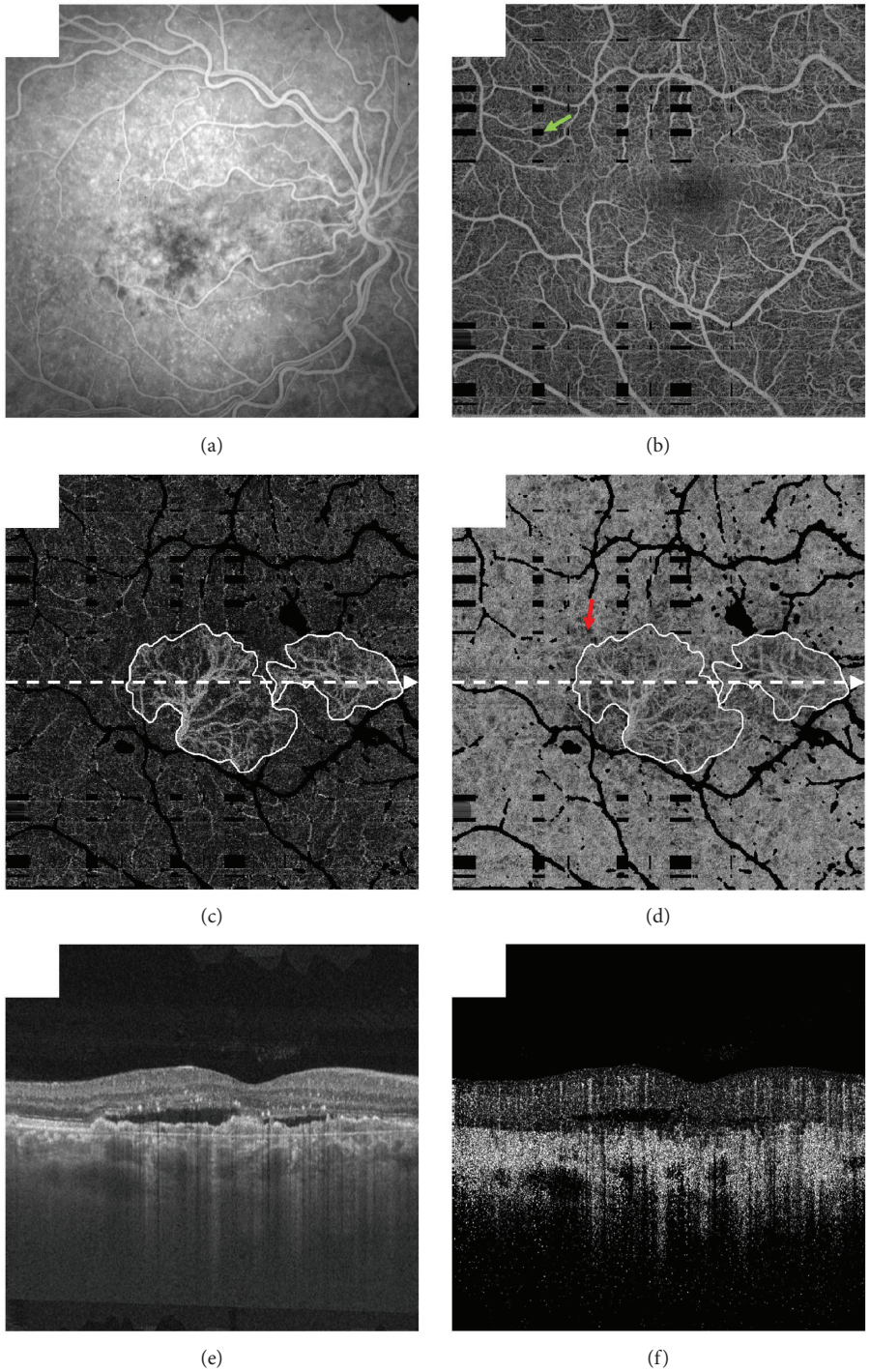

Figure 2: A 65-year-old patient with neovascular age-related macular degeneration (AMD) and treatment-naïve choroidal neovascularization (CNV). (a) Fluorescein angiogram. (b) Projection of the optical coherence tomography (OCT) angiography (OCTA) volume through the depths spanned by the superficial and deep retinal plexuses. The green arrow points to a black rectangular region, which, as a result of patient motion, has absent information (these images were formed by registering and merging orthogonally acquired volumes; at the intersection of motion artifacts in these orthogonal volumes, there is missing information). The field of view is 6 mm × 6 mm. (c) Projection of the OCTA volume through the depths spanned by the CNV lesion; white contours trace the lesion margin. (d) Projection of the OCTA volume from Bruch's membrane to 45 μm below; again, white contours trace the lesion margin, which appears due to projection artifacts. Note that there is choriocapillaris alteration extending beyond the lesion margin (e.g., arrow). (e) OCT B-scan extracted from the position indicated by the dashed white arrows in (c) and (d). (f) OCTA B-scan extracted from the same position. Note that in (b), (c), and (d), projection artifacts from larger overlying retinal vessels have been removed and are shown in black. OCT and OCTA volumes were formed by registering and merging two orthogonally scanned "x-fast" and "y-fast" volumes. Black rectangles in (c) and (d) correspond to intersections of motion in these x-fast and y-fast volumes.

beyond the margins of GA (Figure 1); OCTA was also used to identify choroidal neovascularization (CNV) in two cases that have not been diagnosed with other imaging modalities [25].

4. Choriocapillaris in Neovascular AMD

Regarding the role of choriocapillaris in neovascular AMD, McLeod and colleagues analyzed three postmortem eyes correlating with ocular medical history and demographic information as available and compared them to control eyes. The percentage of RPE coverage and vascular area by choriocapillaris in the regions 1 mm outside of the CNV was 95.9% ± .8% and 39.6% ± 15.9%, respectively. The decrease in choriocapillaris vascular area was evident well beyond the submacular region and in one case extended peripherally 10 mm from the CNV into the equatorial choroid. Compared with aged control eyes, the percentage vascular area in the regions of 1 mm outside of the CNV was significantly reduced, reflecting the loss of interconnecting capillary segments in these regions. There was no significant difference in vessel diameters between the aged control eyes and the viable capillaries in neovascular AMD eyes 1 mm outside the CNV area [11]. Biesemeier and colleagues also analyzed postmortem eyes with neovascular AMD and found that the choriocapillaris was severely affected. In their opinion, the loss of choriocapillaris in neovascular AMD is counteracted by the formation and growth of new blood vessels [12]. In 2016, Seddon and colleagues speculated that hypoxic RPE resulting from reduced blood supply might upregulate production of vascular endothelial growth factor, providing the stimulus for neovascular disease [19]. According to Dryja, these findings suggest that abnormalities of the choriocapillaris may predate piercing of Bruch's membrane by months or years [28].

5. OCTA Documenting Choriocapillaris in Neovascular AMD

Moult and colleagues studied CNV lesions and the underlying choriocapillaris in patients with neovascular AMD, using an ultrahigh-speed swept-source OCTA. They could visualize 16 of 17 eyes with active CNV, corresponding to 94% sensitivity for CNV detection compared to standard fluorescein angiography. In all these 16 eyes, CNV seemed to originate from regions of severe choriocapillaris alteration. These authors also observed that in 14 of these eyes, CNV lesions were surrounded by a region of severe choriocapillaris alteration (Figure 2) [29]. These findings corroborate what McLeod and colleagues found in their study analyzing postmortem eyes [11].

In 2014, Jia and colleagues analyzed choroidal changes in AMD eyes using OCTA and observed that, in all cases, deep choroidal vessels were easier to detect than in control cases; they hypothesized that this could be caused by loss of choriocapillaris associated with AMD. They also found the absence of choriocapillaris in some areas surrounding CNV lesions [30].

6. Conclusion

Significant progress has been made in the understanding of risk factors associated with the development and progression of advanced AMD, either GA or CNV. Nonetheless, the exact underlying mechanisms of tissue damage are still unknown, and the sequence of events involving photoreceptors, RPE, and choriocapillaris loss are still a matter of debate. Pathological changes of the Bruch's membrane, vessel walls, and extracellular deposits must also be considered. In this context, *in vivo* investigation of the choriocapillaris using OCTA may lead to new insights related to underlying disease mechanisms in AMD and may clarify the role of choriocapillaris loss in this vision-threatening disease.

Conflicts of Interest

Eric M. Moult has intellectual property related to variable interscan time analysis. James G. Fujimoto has royalties from intellectual property owned by Massachusetts Institute of Technology and licensed to Carl Zeiss Meditec and Optovue and has stock options with Optovue. Nadia K. Waheed is a consultant for Optovue. Daniela Ferrara is an employee at Genentech Inc., Stock/Stock Options, Roche.

Acknowledgments

Nadia K. Waheed received research support from Carl Zeiss Meditec, Topcon, and Nidek.

References

[1] D. Ferrara, N. K. Waheed, and J. S. Duker, "Investigating the choriocapillaris and choroidal vasculature with new optical coherence tomography technologies," *Progress in Retinal and Eye Research*, vol. 52, pp. 130–155, 2016.

[2] N. D. Wangsa-Wirawan and R. A. Linsenmeier, "Retinal oxygen: fundamental and clinical aspects," *Archives of Ophthalmology*, vol. 121, no. 4, pp. 547–557, 2003.

[3] H. Ida, K. Ishibashi, K. Reiser, L. M. Hjelmeland, and J. T. Handa, "Ultrastructural aging of the RPE-Bruch's membrane–choriocapillaris complex in the D-galactose–treated mouse," *Investigative Ophthalmology & Visual Science*, vol. 45, no. 7, pp. 2348–2354, 2004.

[4] I. A. Pikuleva and C. A. Curcio, "Cholesterol in the retina: the best is yet to come," *Progress in Retinal and Eye Research*, vol. 41, pp. 64–89, 2014.

[5] S. W. Cousins, D. G. Espinosa-Heidmann, A. Alexandridou, J. Sall, S. Dubovy, and K. Csaky, "The role of aging, high fat diet and blue light exposure in an experimental mouse model for basal laminar deposit formation," *Experimental Eye Research*, vol. 75, no. 5, pp. 543–553, 2002.

[6] A. B. Majji, J. Cao, K. Y. Chang et al., "Age-related retinal pigment epithelium and Bruch's membrane degeneration in senescence-accelerated mouse," *Investigative Ophthalmology & Visual Science*, vol. 41, no. 12, pp. 3936–3942, 2000.

[7] Y. Wakatsuki, A. Shinojima, A. Kawamura, and M. Yuzawa, "Correlation of aging and segmental choroidal thickness measurement using swept source optical coherence tomography in healthy eyes," *PLoS One*, vol. 10, no. 12, article e0144156, 2015.

[8] S. Olsen, J. F. Burdick, P. A. Keown, A. C. Wallace, L. C. Racusen, and K. Solez, "Primary acute renal failure ("acute tubular necrosis") in the transplanted kidney: morphology and pathogenesis," *Medicine*, vol. 68, no. 3, pp. 173–187, 1989.

[9] T. S. Olsen, N. F. Wassef, H. S. Olsen, and H. E. Hansen, "Ultrastructure of the kidney in acute interstitial nephritis," *Ultrastructural Pathology*, vol. 10, no. 1, pp. 1–16, 1986.

[10] R. S. Ramrattan, T. L. van der Schaft, C. M. Mooy, W. C. de Bruijn, P. G. Mulder, and P. T. de Jong, "Morphometric analysis of Bruch's membrane, the choriocapillaris, and the choroid in aging," *Investigative Ophthalmology & Visual Science*, vol. 35, no. 6, pp. 2857–2864, 1994.

[11] D. S. McLeod, R. Grebe, I. Bhutto, C. Merges, T. Baba, and G. A. Lutty, "Relationship between RPE and choriocapillaris in age-related macular degeneration," *Investigative Ophthalmology & Visual Science*, vol. 50, no. 10, pp. 4982–4991, 2009.

[12] A. Biesemeier, T. Taubitz, S. Julien, E. Yoeruek, and U. Schraermeyer, "Choriocapillaris breakdown precedes retinal degeneration in age-related macular degeneration," *Neurobiology of Aging*, vol. 35, no. 11, pp. 2562–2573, 2014.

[13] A. O. Edwards, R. Ritter 3rd, K. J. Abel, A. Manning, C. Panhuysen, and L. A. Farrer, "Complement factor H polymorphism and age-related macular degeneration," *Science*, vol. 308, no. 5720, pp. 421–424, 2005.

[14] R. F. Mullins, M. N. Johnson, E. A. Faidley, J. M. Skeie, and J. Huang, "Choriocapillaris vascular dropout related to density of drusen in human eyes with early age-related macular degeneration," *Investigative Ophthalmology & Visual Science*, vol. 52, no. 3, pp. 1606–1612, 2011.

[15] R. F. Mullins, A. D. Dewald, L. M. Streb, K. Wang, M. H. Kuehn, and E. M. Stone, "Elevated membrane attack complex in human choroid with high risk complement factor H genotypes," *Experimental Eye Research*, vol. 93, no. 4, pp. 565–567, 2011.

[16] R. F. Mullins, D. P. Schoo, E. H. Sohn et al., "The membrane attack complex in aging human choriocapillaris: relationship to macular degeneration and choroidal thinning," *The American Journal of Pathology*, vol. 184, no. 11, pp. 3142–3153, 2014.

[17] K. R. Chirco, B. A. Tucker, E. M. Stone, and R. F. Mullins, "Selective accumulation of the complement membrane attack complex in aging choriocapillaris," *Experimental Eye Research*, vol. 146, pp. 393–397, 2016.

[18] S. Zeng, S. S. Whitmore, E. H. Sohn et al., "Molecular response of chorioretinal endothelial cells to complement injury: implications for macular degeneration," *The Journal of Pathology*, vol. 238, no. 3, pp. 446–456, 2016.

[19] J. M. Seddon, D. S. McLeod, I. A. Bhutto et al., "Histopathological insights into choroidal vascular loss in clinically documented cases of age-related macular degeneration," *JAMA Ophthalmology*, vol. 134, no. 11, pp. 1272–1280, 2016.

[20] S. S. Gao, Y. Jia, M. Zhang et al., "Optical coherence tomography angiography," *Investigative Ophthalmology & Visual Science*, vol. 57, no. 9, pp. OCT27–OCT36, 2016.

[21] R. F. Spaide, J. M. Klancnik Jr, and M. J. Cooney, "Retinal vascular layers imaged by fluorescein angiography and optical coherence tomography angiography," *JAMA Ophthalmology*, vol. 133, no. 1, pp. 45–50, 2015.

[22] D. Y. Kim, J. Fingler, R. J. Zawadzki et al., "Optical imaging of the chorioretinal vasculature in the living human eye," *Proceedings of the National Academy of Sciences of the United States of America*, vol. 110, no. 35, pp. 14354–14359, 2013.

[23] T. E. de Carlo, A. Romano, N. K. Waheed, and J. S. Duker, "A review of optical coherence tomography angiography (OCTA)," *International Journal of Retina and Vitreous*, vol. 1, p. 5, 2015.

[24] W. Choi, K. J. Mohler, B. Potsaid et al., "Choriocapillaris and choroidal microvasculature imaging with ultrahigh speed OCT angiography," *PLoS One*, vol. 8, no. 12, article e81499, 2013.

[25] W. Choi, E. M. Moult, N. K. Waheed et al., "Ultrahigh-speed, swept-source optical coherence tomography angiography in nonexudative age-related macular degeneration with geographic atrophy," *Ophthalmology*, vol. 122, no. 12, pp. 2532–2544, 2015.

[26] I. A. Bhutto, D. S. McLeod, T. Hasegawa et al., "Pigment epithelium-derived factor (PEDF) and vascular endothelial growth factor (VEGF) in aged human choroid and eyes with age-related macular degeneration," *Experimental Eye Research*, vol. 82, no. 1, pp. 99–110, 2006.

[27] I. A. Bhutto, T. Baba, C. Merges, D. S. McLeod, and G. A. Lutty, "Low nitric oxide synthases (NOSs) in eyes with age-related macular degeneration (AMD)," *Experimental Eye Research*, vol. 90, no. 1, pp. 155–167, 2010.

[28] T. P. Dryja, "Early insight into neovascular age-related macular degeneration," *JAMA Ophthalmology*, vol. 134, no. 11, pp. 1281-1282, 2016.

[29] E. Moult, W. Choi, N. K. Waheed et al., "Ultrahigh-speed swept-source OCT angiography in exudative AMD," *Ophthalmic Surgery, Lasers and Imaging Retina*, vol. 45, no. 6, pp. 496–505, 2014.

[30] Y. Jia, S. T. Bailey, D. J. Wilson et al., "Quantitative optical coherence tomography angiography of choroidal neovascularization in age-related macular degeneration," *Ophthalmology*, vol. 121, no. 7, pp. 1435–1444, 2014.

Hindawi
Journal of Ophthalmology
Volume 2017, Article ID 3479695, 7 pages
https://doi.org/10.1155/2017/3479695

Research Article

Sensitivity, Specificity, and Limitations of Optical Coherence Tomography Angiography in Diagnosis of Polypoidal Choroidal Vasculopathy

Yi-Ming Huang, Ming-Hung Hsieh, An-Fei Li, and Shih-Jen Chen

Department of Ophthalmology, Taipei Veterans General Hospital, Taipei, Taiwan

Correspondence should be addressed to Shih-Jen Chen; sjchen96@gmail.com

Received 20 August 2017; Accepted 14 November 2017; Published 12 December 2017

Academic Editor: Talisa E. de Carlo

Purpose. To evaluate the sensitivity and specificity of optical coherence tomography angiography (OCTA) in differentiating polypoidal choroidal vasculopathy (PCV) from age-related macular degeneration (AMD). *Methods*. Fundus color photographs, spectral-domain optical coherence tomography, and fluorescein angiography (step 1) and OCTA (step 2) of 50 eyes that had PCV or AMD were presented to two ophthalmologists. The final diagnoses of PCV were masked. Sensitivity and specificity were calculated and compared to the 2-step approach (before and after OCTA) in detecting PCV. The limitations were also evaluated. *Results*. Of the 50 eyes, 31 were PCV and 19 were non-PCV. The sensitivity increased from 69.5% to 90% after OCTA; however, there was no significant improvement in specificity after OCTA. 70.9% of the eyes with PCV had clear or obvious branching vascular nets (BVNs) in OCTA with high sensitivity (97.5%) after OCTA. Contrarily, 29.1% had insignificant BVNs with a low sensitivity (72.5%) after OCTA. 27% of the occult choroidal neovascularization (CNV) cases were overdiagnosed as PCV when OCTA was applied. *Conclusions*. OCTA based on clear BVNs at the choroidal level increased sensitivity of diagnosis of PCV by 20%. However, the false-positive rate also increased in occult CNV. Several limitations for a correct diagnosis of PCV were noted.

1. Introduction

Idiopathic polypoidal choroidal vasculopathy (PCV) was first described by Yannuzzi et al. and is characterized by recurrent subretinal and subretinal pigment epithelium bleeding [1, 2]. PCV seems to be a distinct clinical entity and differs from other types of choroidal neovascularization in age-related macular degeneration (AMD). It is prevalent in Asia, accounting for about 40% to 50% of cases of AMD [2, 3].

The fundus characteristics of PCV include subretinal red or orange nodules and hemorrhagic or exudative pigment epithelial detachment (PED) [1, 4]. Most eyes with PCV display features similar to occult choroidal neovascularization (CNV) in fluorescein angiography (FA) [5]. Spectral-domain optical coherence tomography (SD-OCT) is another useful tool based on features of sharp PED and double-layer signs at the retinal pigment epithelium [6]. However, indocyanine green angiography (ICGA) is the gold standard tool for the diagnosis of PCV, where polypoidal dilation and choroidal branching vascular nets (BVNs) are observed [7].

OCT angiography (OCTA) is a new imaging tool used to diagnose PCV. The polyps appear as hypoflow round structures, whereas the BVNs are detected as hyperflow vascular networks [8]. However, whether OCTA can help differentiate PCV with various clinical signs that resemble AMD is unknown. [9] Therefore, the aim of this study was to evaluate the sensitivity, specificity, and limitations of OCTA in distinguishing PCV from AMD in clinical practice.

2. Patients and Methods

We retrospectively collected images of patients who had macular subretinal fluid with or without pigment epithelial detachment (PED) or hemorrhage attributable to either PCV or AMD (occult CNV, retinal angiomatous proliferation, classic CNV, and drusenoid PED and mixed with both occult and classic CNV) from January 2015 to February 2016 in a tertiary medical center in Taiwan. The images included color fundus photographs, SD-OCT (Optovue, Fremont, CA), OCTA (Avanti; Optovue, Fremont, CA), FA, and ICGA (Heidelberg Engineering Inc., Heidelberg, Germany). Patients with retinal vascular occlusion, myopic CNV, and other secondary CNVs, diabetic retinopathy, and central serous chorioretinopathy were excluded. Poor quality images such as those with a hazy medium or poor fixation of OCTA were also excluded. The patients with a history of treatment including photodynamic therapy (PDT) or intravitreal injections of antivascular endothelial growth factor (VEGF) therapy were not excluded. The OCTA images were not further refined or modified even if autosegmentation was not perfectly aligned, and the cross-sectional picture with the segmentation line was provided (Figure 1, bottom). The diagnosis of PCV was confirmed by ICGA as the presence of polyps with or without BVNs. The eligible images were then masked and tested by one senior retina specialist and one retinal fellow for the diagnosis masked to the results of ICGA.

At the first step, one color image of the macula, three FA images (early, mid, and late phases), and two (horizontal and vertical) cross-sectional SD-OCT images of all cases were provided to the two graders (Figure 1) who were then asked if the diagnosis was PCV or non-PCV. Cases that could not be determined with the provided images were classified as being non-PCV. In the second step, the graders were asked to make a diagnosis again after presenting the OCTA images. The OCTA images include four images (superficial retina, deep retina, retinal pigment epithelium, and choriocapillary level; Figure 1). Sensitivity and specificity were calculated and compared between the 2-step results (before and after OCTA) and the gold standard of ICGA. Differences in diagnoses between the two graders were also compared to evaluate the diagnostic accuracy between the experienced and nonexperienced retinal doctors. Images with false-positive and false-negative results were evaluated and compared to identify the limitations of OCTA for the diagnosis of PCV.

Statistical analyses were performed with PASW Statistics for Windows, Version 18.0 (SPSS Inc., Chicago, Illinois, USA), using McNemar chi-square test. $P < .05$ was considered statistically significant.

3. Results

Among the 50 eyes, 31 were confirmed to have PCV and 19 to not have PCV by ICGA (11 with occult CNV, four with classic CNV, one with mixed type, two with a retinal angiomatous proliferation, and one with drusenoid PED). In comparison, an average of 32 eyes were diagnosed as PCV and 18 as non-PCV by the two graders. An average of 87.5% (28/32) were true positive, 12.5% (4/32) were false positive, 83.4% (15/18) were true negative, and 16.6% (3/18) were false negative.

The sensitivity increased from 69.5% (71% and 68%, resp.) to 90% for both graders from step 1 to step 2 after OCTA (Table 1). Figure 1 shows multimodal images of a true-positive PCV case for both graders. A mild decrease (from 84% to 74%) in specificity was noted for the senior retina specialist after OCTA due to an increased false-positive rate. However, for the retinal fellow, the specificity improved from 68% to 84%. Overall, the sensitivity significantly improved after OCTA ($p = 0.046$); however, the specificity did not ($p = 0.856$).

Six PCV cases (three each for the retina specialist and fellow) were misdiagnosed as being non-PCV (false negative) after providing OCTA images, all of which had unclear or insignificant BVNs in the OCTA images. Therefore, we further classified all of the PCV cases into two groups based on whether or not they had clear and obvious BVNs in the OCTA images. The results showed that 70.9% of the PCV cases (22/31) had clear or obvious BVNs and that this feature was the most sensitive to make an accurate diagnosis (sensitivity 97.5%). On the other hand, 29.1% of the PCV cases (9/31) had insignificant BVNs, all of which had a lower sensitivity of 72.5%.

Among the 11 cases of occult CNV, an average 27.2% (four for the retina specialist and two for the fellow) were overdiagnosed as PCV after OCTA. Other false-positive cases included one mixed-type CNV and one classic CNV. All false-positive cases had a BVN-like shape in OCTA.

4. Discussion

Our results showed that after providing color, FA, and cross-sectional SD-OCT images, OCTA increased the sensitivity of a diagnosis of PCV from 69.5% to 90% ($p < 0.05$). This increase in sensitivity was mainly due to the presence of BVNs in OCTA. Without manually adjusting for the segmentation line, BVNs were found in 70% and polyps in only 42% of our 31 cases with PCV. Unlike BVNs that resides within the Bruch's membrane, polyps are located on a more anterior and variable plane above BVNs and are identified in OCTA in less than half of cases [10]. In addition, the low flow of polyps and hence low signal in OCTA can decrease the detection of polyps [10]. With manual adjustments for the segmentation line, the polyp detection rate can be as high as 85%, whereas the detection rate of BVNs remains around 70% in OCTA compared to ICGA [11]. Therefore, BVNs are a more ready and critical feature than polyps for the diagnosis of PCV in OCTA.

In addition, if OCTA does not show BVNs, the diagnosis will be possibly undetermined, especially for cases with an organized hemorrhage, large PED, extramacular polyps, and polyps without BVNs as in our study (Figure 2). On the other hand, polyps can regress after anti-VEGF treatment, photodynamic therapy, or a combination of therapies [12]. In the false-positive cases with discernible vascular nets in OCTA but no polyps in ICGA, 75% (6/8) of the cases had

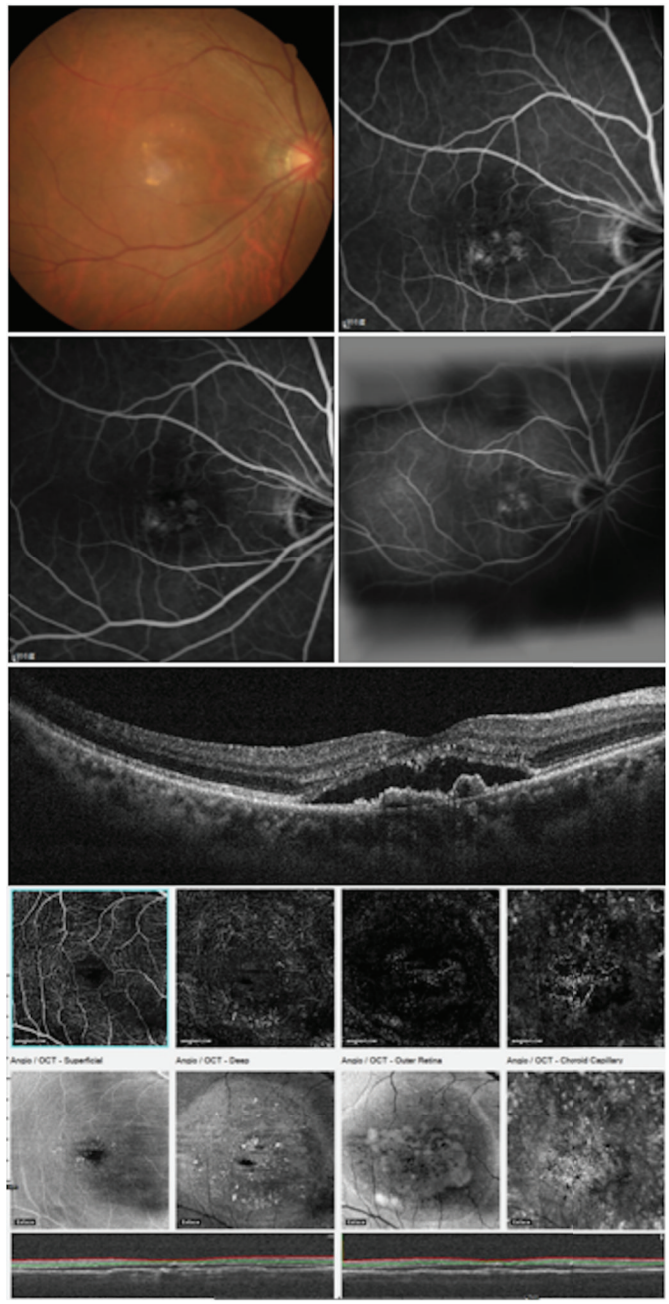

Figure 1: Two steps of multimodal evaluation of an example. In the first step, one color picture of the macula (top left), early (top right), mid, and late phases (the second row, left to right) of fluorescein angiography, and spectral-domain optical coherence tomography images (the third row) of all cases were given to the two graders. In the second step, the optical coherence tomography angiography (OCTA) images including four images at the superficial retina, deep retina, outer retina, and choriocapillary level were provided (the fourth to sixth rows). The two graders then made a diagnosis of polypoidal choroidal vasculopathy (PCV) or non-PCV in each step.

Table 1: Sensitivity and specificity before and after optical coherence tomography angiography (OCTA) in the diagnosis of polypoidal choroidal vasculopathy.

	Sensitivity			Specificity		
	Retina specialist	Fellow	Average	Retina specialist	Fellow	Average
Before OCTA	71%	68%	69.5%	84%	68%	76%
After OCTA	90%	90%	90%	74%	84%	79%
p value		*0.046			0.856	

*$p < 0.05$.

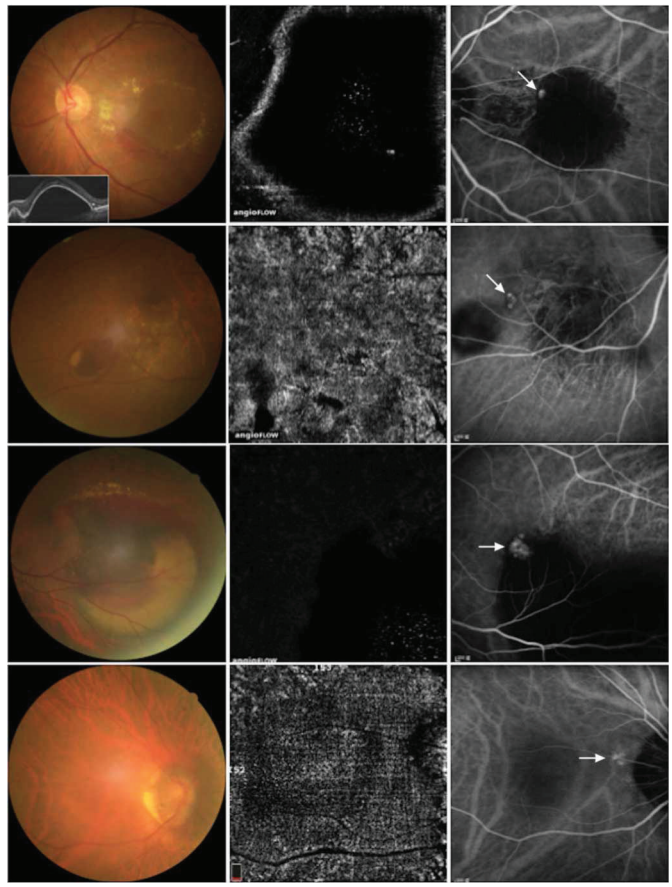

Figure 2: Four limitations of optical coherence tomography angiography (OCTA) for a diagnosis of polypoidal choroidal vasculopathy. Left: color fundus; middle: OCTA; right: indocyanine green angiography. The first row: large pigment epithelial detachments (PEDs). The second row: extramacular polyps with hemorrhage or exudation. The third row: massive organized blood and exudation. The fourth row: polyps without significant branching vascular nets.

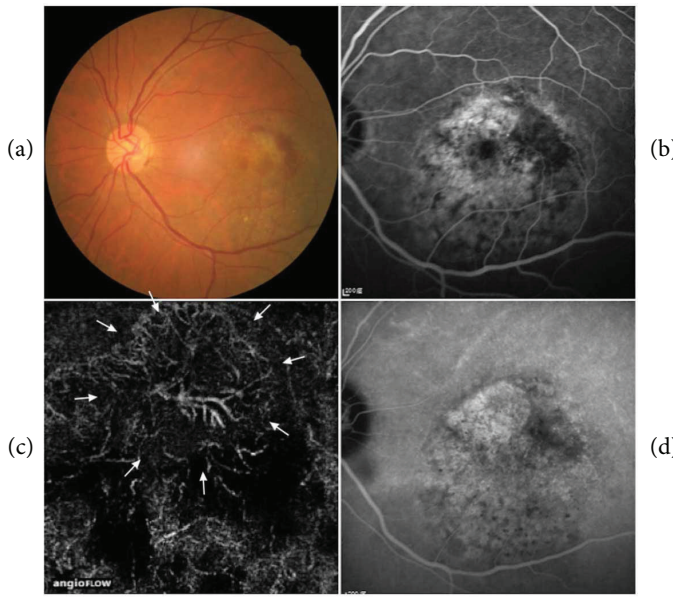

Figure 3: Occult choroidal neovascularization (occult CNV) could be misdiagnosed as idiopathic polypoidal choroidal vasculopathy by optical coherence tomography angiography (OCTA). Color fundus image showed a retinal hemorrhage (a), and fluorescein angiography showed an occult CNV leakage pattern (b). OCTA revealed a branching vascular net-like shape (arrows) (c). However, indocyanine green angiography did not detect any polyps (d).

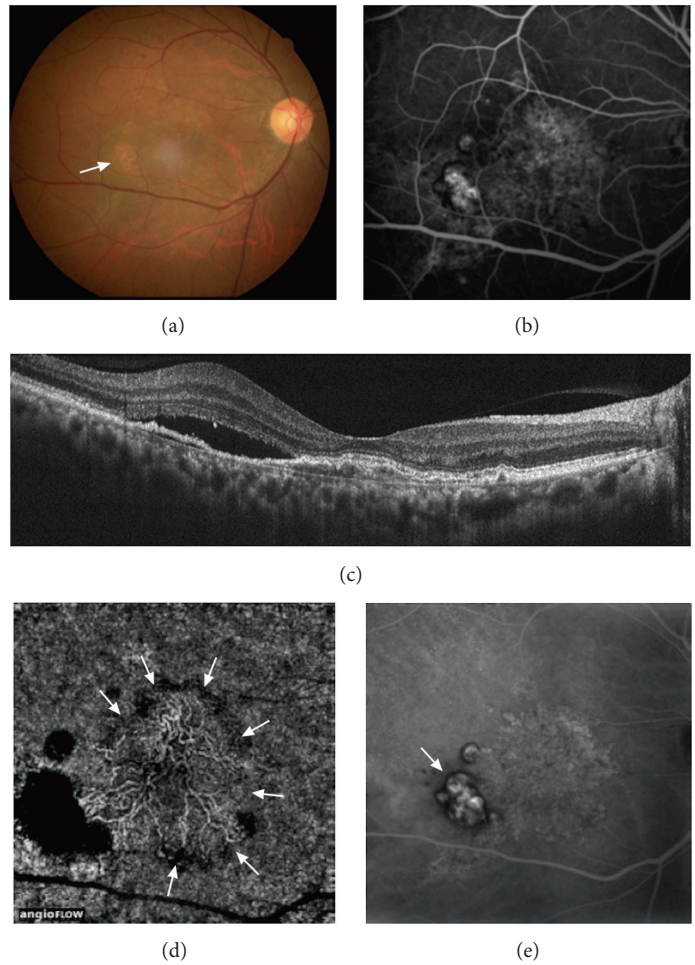

Figure 4: True-positive case of polypoidal choroidal vasculopathy (PCV). Subretinal orange nodules in a color image (arrow) (a), localized pigment epithelial detachments (PEDs) with delayed leakage of an occult choroidal neovascularization pattern in fluorescein angiography, (b) and subretinal fluid in spectral-domain optical coherence tomography (c) were noted. Optical coherence tomography angiography showed branching vascular nets (arrows) with surrounding PEDs at a choroidal level, but no significant polyps (d). Indocyanine green angiography confirmed polyps beneath the PEDs (arrow) and the diagnosis of PCV (e).

previously received intravitreal injections of anti-VEGF, and two of six patients had a history of PCV in their fellow eyes. Figure 3 shows an occult case of CNV misdiagnosed as PCV after OCTA because of a BVN-like structure at the choroidal level. Among these six cases, three had shallow irregular PEDs with a double-layer sign, two had a large PED, and one had hemorrhagic PEDs. Therefore, the possibility of regressed polyps in these patients cannot be ruled out due to previous treatments [13].

As shown in a typical case (Figure 4), several features help to diagnose PCV, including orange-red nodules in color photography, an occult CNV leakage pattern or serous PED in FA, and a double-layer sign with a sharp elevation in PED in cross-sectional SD-OCT. Salvo et al. used SD-OCT to diagnose PCV and reported sensitivity and specificity rates of higher than 90% [6]. However, they included only patients with PCV and occult CNV, while we included other subtypes of AMD and thus had lower sensitivity of 69.5% and specificity of 76%. Several features help to diagnose PCV as shown in the typical case in Figure 4. After OCTA, the sensitivity was increased to 90% based on BVNs. We therefore propose a diagnostic flow chart for PCV as shown in Figure 5. By fundus color, FA, SD-OCT, and additional OCTA, at least 42% (positive of both polyps and BVNs in OCTA in our series) of the suspected patients with PCV did not need to undergo ICGA.

Dansingani et al. also reported that in the eyes with pachychoroid features and shallow irregular PEDs, OCTA had a greater diagnostic value for type 1 neovascularization than FA and ICGA [14]. Furthermore, OCTA has also been reported to identify treatment-naive quiescent CNV to guide return visits and decisions regarding treatment [15]. Therefore, OCTA may be a useful follow-up tool for silent or active type 1 CNV.

There are several limitations to this study, including the small number of patients, autosegmentation of OCTA was not perfect without manual adjustments, and some (60%) cases had been treated before, which increased the difficulty of the diagnosis of PCV. However, we believed that the OCTA images were more representative

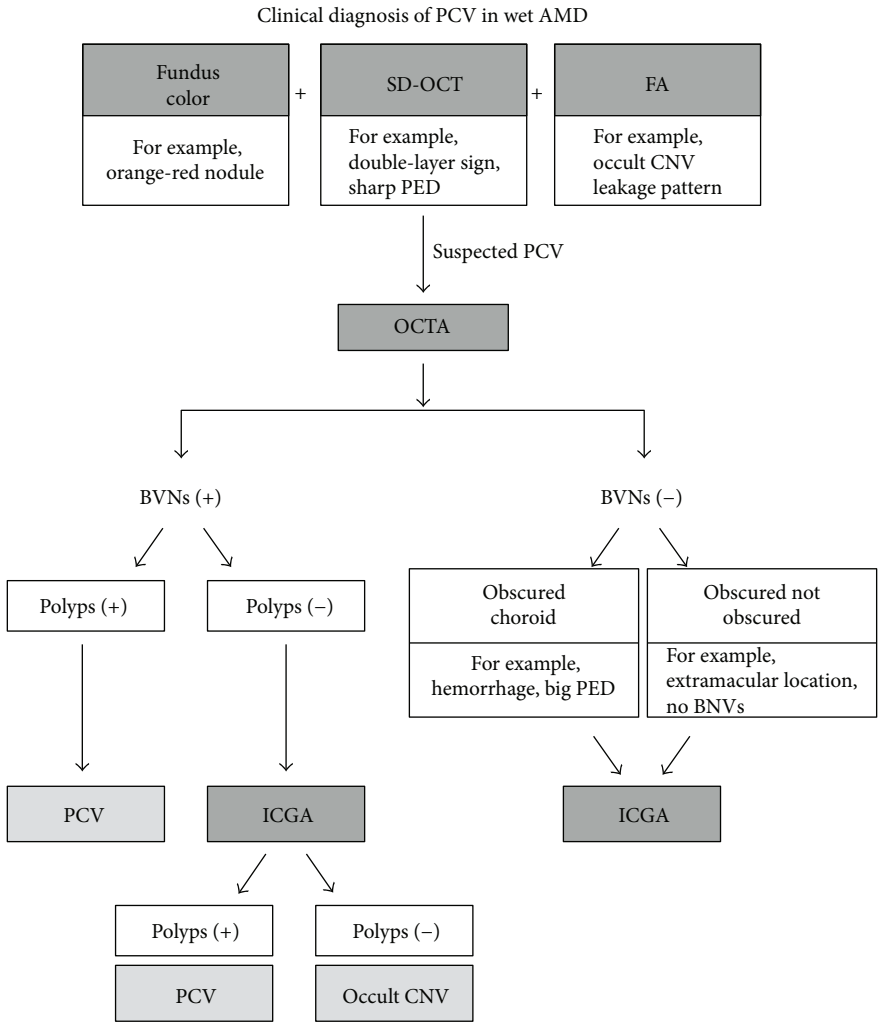

Figure 5: Clinical diagnosis of idiopathic polypoidal choroidal vasculopathy (PCV) in age-related macular degeneration (AMD) with optical coherence tomography angiography (OCTA). If the patient is suspected of having idiopathic polypoidal choroidal vasculopathy (PCV), OCTA is the next exam. With obvious branching vascular nets (BVNs) in OCTA, further polyp detection is the next sign for a diagnosis of PCV; if not, further indocyanine green angiography (ICGA) is required for cases without BVNs or further polyps in OCTA. FA: fluorescein angiography; PEDs: pigment epithelial detachments; SD-OCT: spectral-domain optical coherence tomography.

of daily clinical practice and that postimage manual adjustments or processing was not available before the introduction of the automated retinal layer segmentation algorithm. [16]

In conclusion, by identifying BVNs in OCTA at a choroidal level, the sensitivity of diagnosing PCV with color, SD-OCT, and FA images increased by 20%. Future studies should investigate how well OCTA can identify polyps with more sophisticated analysis of imaging data in a cohort of patients with AMD and increase the diagnostic accuracy of PCV compared to ICGA.

Conflicts of Interest

The authors declare that there is no conflict of interest regarding the publication of this paper.

References

[1] L. A. Yannuzzi, J. Sorenson, R. F. Spaide, and B. Lipson, "Idiopathic polypoidal choroidal vasculopathy (IPCV)," *Retina*, vol. 10, no. 1, pp. 1–8, 1990.

[2] A. P. Ciardella, I. M. Donsoff, S. J. Huang, D. L. Costa, and L. A. Yannuzzi, "Polypoidal choroidal vasculopathy," *Survey of Ophthalmology*, vol. 49, no. 1, pp. 25–37, 2004.

[3] S. Honda, W. Matsumiya, and A. Negi, "Polypoidal choroidal vasculopathy: clinical features and genetic predisposition," *Ophthalmologica*, vol. 231, no. 2, pp. 59–74, 2014.

[4] M. Uyama, M. Wada, Y. Nagai et al., "Polypoidal choroidal vasculopathy: natural history," *American Journal of Ophthalmology*, vol. 133, no. 5, pp. 639–648, 2002.

[5] B. A. Lafaut, A. M. Leys, B. Snyers, F. Rasquin, and J. J. De Laey, "Polypoidal choroidal vasculopathy in Caucasians," *Graefe's Archive Clinical and Experimental Ophthalmology*, vol. 238, no. 9, pp. 752–759, 2000.

[6] G. De Salvo, S. Vaz-Pereira, P. A. Keane, A. Tufail, and G. Liew, "Sensitivity and specificity of spectral-domain optical coherence tomography in detecting idiopathic polypoidal choroidal vasculopathy," *American Journal of Ophthalmology*, vol. 158, no. 6, pp. 1228–1238.e1, 2014.

[7] R. F. Spaide, L. A. Yannuzzi, J. S. Slakter, J. Sorenson, and D. A. Orlach, "Indocyanine green videoangiography of idiopathic polypoidal choroidal vasculopathy," *Retina*, vol. 15, no. 2, pp. 100–110, 1995.

[8] M. Srour, G. Querques, O. Semoun et al., "Optical coherence tomography angiography characteristics of polypoidal choroidal vasculopathy," *The British Journal of Ophthalmology*, vol. 100, no. 11, pp. 1489–1493, 2016.

[9] A. N. Stangos, J. S. Gandhi, J. Nair-Sahni, H. Heimann, C. J. Pournaras, and S. P. Harding, "Polypoidal choroidal vasculopathy masquerading as neovascular age-related macular degeneration refractory to ranibizumab," *American Journal of Ophthalmology*, vol. 150, no. 5, pp. 666–673, 2010.

[10] M. Inoue, C. Balaratnasingam, and K. B. Freund, "Optical coherence tomography angiography of polypoidal choroidal vasculopathy and polypoidal choroidal neovascularization," *Retina*, vol. 35, no. 11, pp. 2265–2274, 2015.

[11] T. Tomiyasu, M. Nozaki, M. Yoshida, and Y. Ogura, "Characteristics of polypoidal choroidal vasculopathy evaluated by optical coherence tomography angiography," *Investigative Ophthalmology & Visual Science*, vol. 57, no. 9, pp. OCT324–OCT330, 2016.

[12] A. Koh, W. K. Lee, L. J. Chen et al., "Everest study: efficacy and safety of verteporfin photodynamic therapy in combination with ranibizumab or alone versus ranibizumab monotherapy in patients with symptomatic macular polypoidal choroidal vasculopathy," *Retina*, vol. 32, no. 8, pp. 1453–1464, 2012.

[13] T. Wakabayashi, F. Gomi, M. Sawa, M. Tsujikawa, and Y. Tano, "Marked vascular changes of polypoidal choroidal vasculopathy after photodynamic therapy," *The British Journal of Ophthalmology*, vol. 92, no. 7, pp. 936–940, 2008.

[14] K. K. Dansingani, C. Balaratnasingam, M. A. Klufas, D. Sarraf, and K. B. Freund, "Optical coherence tomography angiography of shallow irregular pigment epithelial detachments in pachychoroid spectrum disease," *American Journal of Ophthalmology*, vol. 160, no. 6, pp. 1243–1254.e2, 2015.

[15] A. Carnevali, M. V. Cicinelli, V. Capuano et al., "Optical coherence tomography angiography: a useful tool for diagnosis of treatment-naïve quiescent choroidal neovascularization," *American Journal of Ophthalmology*, vol. 169, pp. 189–198, 2016.

[16] M. Zhang, J. Wang, A. D. Pechauer et al., "Advanced image processing for optical coherence tomographic angiography of macular diseases," *Biomedical Optics Express*, vol. 6, no. 12, pp. 4661–4675, 2015.

Hindawi
Journal of Ophthalmology
Volume 2017, Article ID 6913980, 10 pages
https://doi.org/10.1155/2017/6913980

Research Article

Detection of Silent Type I Choroidal Neovascular Membrane in Chronic Central Serous Chorioretinopathy Using En Face Swept-Source Optical Coherence Tomography Angiography

Magdy Moussa,[1,2] Mahmoud Leila,[3] Hagar Khalid,[1,2] and Mohamed Lolah[4]

[1]*Ophthalmology Department, Faculty of Medicine, Tanta University, Tanta, Egypt*
[2]*MEDIC Eye Center, Tanta, Egypt*
[3]*Retina Department, Research Institute of Ophthalmology, Giza, Egypt*
[4]*Ophthalmology Department, Faculty of Medicine, Alexandria University, Alexandria, Egypt*

Correspondence should be addressed to Magdy Moussa; magdymoussa60@gmail.com

Received 30 August 2017; Accepted 30 October 2017; Published 4 December 2017

Academic Editor: Talisa E. de Carlo

Purpose. To evaluate the efficacy of SS-OCTA in the detection of silent CNV secondary to chronic CSCR compared to that of FFA and SS-OCT. *Patients and Methods*. A retrospective observational case series reviewing the clinical data, FFA, SS-OCT, and SS-OCTA images of patients with chronic CSCR, and comparing the findings. SS-OCTA detects the CNV complex and delineates it from the surrounding pathological features of chronic CSCR by utilizing the blood flow detection algorithm, OCTARA, and the ultrahigh-definition B-scan images of the retinal microstructure generated by swept-source technology. The bivariate correlation procedure was used for the calculation of the correlation matrix of the variables tested. *Results*. The study included 60 eyes of 40 patients. Mean age was 47.6 years. Mean disease duration was 14.5 months. SS-OCTA detected type 1 CNV in 5 eyes (8.3%). In all 5 eyes, FFA and SS-OCT were inconclusive for CNV. The presence of foveal thinning, opaque material beneath irregular flat PED, and increased choroidal thickness in chronic CSCR constitutes a high-risk profile for progression to CNV development. *Conclusion*. Silent type 1 CNV is an established complication of chronic CSCR. SS-OCTA is indispensable in excluding CNV especially in high-risk patients and whenever FFA and SS-OCT are inconclusive.

1. Introduction

Theories of pathogenesis of central serous chorioretinopathy (CSCR) suggest that the retinal pigment epithelium- (RPE-) Bruch's membrane complex is compromised by shear stress caused by accumulating fluid that egresses from the choroidal circulation due to choroidal vascular hyperpermeability and consequent increased choroidal hydrostatic pressure [1–6]. Chronic CSCR is defined as persistent symptoms for at least 6 months from the onset of acute attack or persistent subretinal fluid associated with retinal pigment epitheliopathy and leaking points on fundus fluorescein angiography (FFA) [7]. Protracted contact between tenacious subretinal fluid and the RPE induces a spectrum of pathological changes in the RPE cell layer that includes atrophy, hypertrophy, and hyperplasia eventually leading to RPE cell dysfunction. The spectrum is known collectively as sick RPE syndrome and is considered the hallmark of chronic CSCR [7, 8]. The coexistence of choroidal vascular hyperpermeability, breached RPE-Bruch's complex, and chronic course purportedly incites the development of choroidal neovascular (CNV) membrane [9–12]. Detection of type 1 CNV secondary to chronic CSCR could be challenging using conventional angiography techniques, namely, FFA and indocyanine angiography (ICG), due to overlapping fluorescein leakage patterns and ICG fluorescence patterns of both pathologies [13–15]. On the other hand, optical coherence tomography (OCT) could yield inconclusive results even when deploying modern versions that provide ultrahigh-definition images acquired by swept-source (SS-OCT) technology. The reason is that pathological features associated with chronic CSCR include the thickened irregular RPE layer, in addition to subretinal

deposits composed of shed photoreceptor outer segments and subretinal and sub-RPE lipoproteinaceous clumps derived from long-standing serous fluid. These features could have backscattering light intensity properties that are similar to those of the neovascular or fibrovascular components of the CNV, rendering both pathologies virtually indistinguishable from each other [13, 16]. The recently introduced swept-source OCT angiography (SS-OCTA) helped disentangle the perplexity of CNV underlying chronic CSCR by relaying information on the neovascular network that is unique for CNV. The SS-OCTA technology incorporates a blood flow detection algorithm, OCTARA, that is capable of visualizing the superficial retinal capillaries and foveal avascular zone, inner and outer retinal vascular plexuses, choriocapillaris, and larger choroidal vasculature in vivo without the need for contrast injection [17]. In addition, SS-OCTA utilizes the features of merged SS-OCT technology including long-wavelength (1050 nm) scanning light, less susceptibility-to-sensitivity roll-off, and ultrahigh-speed image acquisition. These features enabled deeper penetration and superior axial resolution and generation of ultrahigh-definition B-scan images of the retinal microstructure [18–22]. Thus, SS-OCTA could detect the CNV complex and delineate it from the surrounding pathological features of chronic CSCR particularly where FFA and SS-OCT alone reveal inconclusive results. This notion has been corroborated by several studies that reported the use of OCTA technology to detect CNV secondary to chronic CSCR, which was unrevealed by conventional imaging modalities [9, 11, 13, 23]. The current study aims to evaluate the efficacy of SS-OCTA in the detection of silent CNV secondary to chronic CSCR and to further compare the results with those of conventional FFA and with those of SS-OCT.

2. Patients and Methods

2.1. Patients. This is a retrospective observational case series in which we reviewed the clinical data, FFA, SS-OCT, and SS-OCTA images of all consecutive patients diagnosed with chronic CSCR in a private practice from September 2015 to June 2017, and compared the findings.

2.2. Inclusion Criteria. All patients included in the study had typical features of chronic CSCR on biomicroscopic examination (diffuse retinal pigment epitheliopathy, neurosensory and/or RPE detachment, and subretinal deposits), on FFA (early leaking point(s) at the level of the RPE, pooling of dye in single or multiple areas of PED, and alternating areas of hyper- and hypofluorescence caused by RPE alteration), and on SS-OCT (neurosensory detachment, solitary or multiple PED(s), irregularly thickened RPE layer, hyperreflective amorphous subretinal and/or sub-RPE deposits, and increased choroidal thickness). Patients were required to have a disease duration of more than 6 months to be eligible for the study. All recruited patients were treatment naïve at the time of enrollment.

2.3. Exclusion Criteria. The exclusion criteria included concomitant ocular diseases that could cause localized serous detachment of the macula, such as diabetic retinopathy, vascular occlusion, age-related macular degeneration, and optic pit maculopathy, or hereditary ocular diseases and patients presenting initially with documented concomitant choroidal neovascularization or media opacity that was dense enough to preclude sufficient image quality for reliable interpretation. Any patient who received treatments for chronic CSCR that might have altered the features of the disease or masked preexisting CNV including laser treatment, anti-VEGF agents, photodynamic therapy (PDT), or mineralocorticoids were excluded from the study.

3. Methods

3.1. FFA. FFA images were obtained using a Topcon TRC 50DX fundus camera (Topcon Corporation, Tokyo, Japan).

3.2. SS-OCT. SS-OCT images were acquired using the DRI OCT Triton machine version 10.11 (Topcon Corporation, Tokyo, Japan). The machine incorporates the swept-source technology, which utilizes an infrared (1050 nm) laser source and analog-to-digital acquisition mode that minimizes variation in sensitivity with depth (sensitivity roll-off) allowing deeper penetration and superior axial resolution. The infrared laser operates at a scanning speed of 100,000 A-scans/second. This ultrahigh acquisition speed enables dense raster scanning to acquire high volumetric data generating ultrahigh-definition B-scan images. The routine protocol used for scanning each patient consisted of a radial scan consisting of 12 radial lines (1024 A-scans × 12) (each line is 9 mm or 12 mm in length to include the entire lesion) centered onto the fovea, horizontal and vertical line scans (1024 A-scans, 9.00 mm) centered onto the fovea, and a 3D scan (512 A-scans × 256 scan lines). The central foveal thickness (CFT) value was obtained from a macular thickness map displayed as ETDRS grids. The choroidal thickness in the subfoveal area was measured using calipers from the outer boundary of the RPE to the inner boundary of the sclera.

3.3. SS-OCT Angiography (SS-OCTA) and OCTARA Algorithm. OCTARA (optical coherence tomography angiography ratio analysis) (Topcon Corporation, Tokyo, Japan) is a blood flow detection algorithm that uses decorrelation motion contrast between rapidly repeated SS-OCT B-scans to visualize blood flow in vivo without the need for contrast injection. This OCTA implement benefits from being merged with SS-OCT technology as the deeper penetration of the infrared wavelength allows segmentation of different layers of the ocular fundus. In case CNV is present, it is possible to generate depth-resolved images of the neovascular lesion and its location in relation to the RPE-Bruch's-choriocapillaris complex. Acquired scans are displayed simultaneously as separate en face images of 3 retinal layers (superficial capillary plexus, deep capillary plexus, and outer retina) and the choriocapillaris. It is worthy of note that the OCTARA algorithm generates OCTA images by registering B-scan repetition at each scan location and then computing a ratio-based result between corresponding image pixels. This method preserves the integrity of the OCT spectrum

and does not result in compromised axial resolution, an inherent disadvantage of other OCTA technologies.

3.4. Image Acquisition. OCTA acquisition protocol in the macular region consisted of a $3 \times 3\,mm^2$ area centered onto the fovea for maximum resolution of the lesion examined. Whenever the lesion extended beyond the image border, a $4.5 \times 4.5\,mm^2$, $6 \times 6\,mm^2$, or $9 \times 9\,mm^2$ area was used to include the entire extent of the lesion. By default, the integrated software (IMAGEnet 6 ophthalmic data system) deploys automated segmentation to delineate the lesion and its location in relation to the RPE-Bruch's membrane-choriocapillaris complex. In cases of significant disorganization of retinal layers as in large PED or sizeable subretinal fluid or deposits, the integrated automated segmentation feature failed to detect the correct boundaries of the lesion and we had to resort to manual adjustment of the segmentation slab. To perform manual segmentation, the operator manually places two segmentation lines at sequential depths guided by corresponding SS-OCT images to reveal the maximum extent of the lesion and its actual location.

3.5. Color Coding. The SS-OCTA software generates a color-coded flow density map of the retinal superficial and deep capillary plexuses, the outer retina, and the choriocapillaris that could be displayed individually or as a composite montage of all 4 layers. Bright red color represents areas of dense vascular flow, whereas dark blue represents areas devoid of blood flow. Intermediate color shades represent variable grades of flow. This density map helps to highlight abnormal vascular flow within a neovascular complex relative to the surrounding avascular outer retina or the choriocapillaris.

3.6. SS-OCTA Interpretation. The SS-OCTA criteria for active CNV were defined as interlacing tiny capillaries, extensive arborization, vascular anastomosis, and looping, whereas the criteria for inactive CNV were defined as large linear vessels widely separated by dark spaces with no or minimal anastomosis and the presence of single or multiple feeder vessels supplying the neovascular complex.

All three imaging modalities were performed on the same day. Patient selection for enrollment and image interpretation were undertaken by an experienced retina specialist (MM). The study was performed in accordance with the tenets of the Declaration of Helsinki of 1975 (the 2013 revision). All patients received thorough explanation of the procedures entailed in the study and signed an informed consent before undertaking any of the imaging modalities described above. The consent included a statement that authorized the authors to publish patients' photos and data for research purposes in an anonymous manner that does not allow identification of the patient.

3.7. Statistical Analysis. For the calculation of the correlation matrix, we used the bivariate correlation procedure that computes Pearson's correlation coefficient. Correlation measures how variables are related. Two variables can be perfectly related, but if the relationship is not linear, Pearson's correlation coefficient is not an appropriate statistic. The results of the r value were checked on the r table to find out the significant level. Correlation coefficient $(R) = (N \sum XY - \sum X \sum Y)/[\mathrm{SQR}\ (N\sum X^2 - (\sum X)^2)\ (N\sum Y^2 - (\sum Y)^2)]$, where X is the independent variable and Y is the dependent variable. The coefficient of determination (R^2) procedure computes relative contribution of independent variable (X) to the dependent variable (Y).

Table 1: Baseline patients' characteristics.

Baseline characteristics	N (%)
Male	34 (85)
Female	6 (15)
Age (years)	
<40	9 (22.5)
40–50	16 (40)
51–60	7 (17.5)
>60	8 (20)
Baseline BCVA (logMar)	
0–0.1	18 (30)
>0.1–0.3	14 (23.3)
>0.3–1	26 (43.3)
>1	2 (3.3)
Laterality	
Unilateral	20 (50)
Bilateral	20 (50)
Disease duration (months)	
6–12	25 (41.6)
>12–18	26 (43.3)
>18	9 (15)

4. Results

4.1. Patients' Characteristics. The study included 60 eyes of 40 patients (34 men and 6 women) with a mean age of 47.6 years (range 26–66; SD 10.5). Chronic CSCR was bilateral in 20 patients (50%). Mean best-corrected visual acuity (BCVA) was 0.4 logMAR (range 0–1.5 logMAR; SD 0.4). Mean disease duration was 14.5 months (range 6–28 months; SD 6) (Table 1).

4.2. Chronic CSCR Features. Residual subretinal fluid was present in 44 eyes (73.3%). In the remaining 16 eyes (27%), subretinal fluid was more extensive in the form of neurosensory detachment. Mean CFT by SS-OCT was 242 μ (range 102-725 μ; SD 110). Subretinal deposits were encountered in 39 eyes (65%). PED was encountered in 55 eyes (92%), of which 46 eyes (84%) had the thick flat irregular variant, whereas 9 eyes (16.3%) had the dome-shaped smooth regular variant. Sub-RPE deposits were detected in 35 (58%) eyes. Disrupted outer retinal layers including external limiting membrane (ELM) and inner segment/outer segment (IS/OS) junction were present in 49 eyes (82%). Foveal thinning was detected in 14 eyes (23%). One patient (1.6%) had choroidal excavation. Choroidal thickening with dilated choroidal vessels were detected in 50 (83%) out of 60 eyes included in the study. Mean subfoveal choroidal thickening

Table 2: Chronic CSCR features in the study population.

Chronic CSCR features	*N* (%)
Residual subretinal fluid	44 (73.3)
Neurosensory detachment	16 (27)
PED (total number of eyes)	55 (92)
(i) Flat irregular PED	46 (84)
(ii) Dome-shaped smooth PED	9 (16.3)
Disrupted ELM-IS/OS layers	49 (82)
Foveal thinning	14 (23.3)
Choroidal excavation	1 (1.6)
Mean choroidal thickening (μ)	
(i) Affected eye(s)	412
(ii) Contralateral normal eye(s)	354

CSCR: central serous chorioretinopathy; ELM: external limiting membrane; IS/OS: inner segment/outer segment junction; PED: pigment epithelial detachment; μ: micron.

was 412 μ (range 196–737 μ; SD 113). Mean subfoveal choroidal thickening of the contralateral eye of the 20 patients who had unilateral chronic CSCR was 354 μ (range 235–526 μ; SD 86) (Table 2).

4.3. Silent Type 1 Choroidal Neovascularization. SS-OCTA imaging detected type 1 CNV formation in 5 (8.3%) out of 60 eyes; one of these eyes had polypoidal choroidal vasculopathy (PCV) variant of type 1 CNV. In all 5 cases, FFA and SS-OCT findings were inconclusive for CNV.

4.4. Correlation between Chronic CSCR Features and CNV Development. For statistical analysis, the study population was classified into 2 groups. Group I included 55 eyes that were not complicated with CNV. Group II included 5 eyes that developed CNV. Subsequently, we proceeded to the assessment of the contribution of chronic CSCR features to the CNV-free status in group I and to the development of CNV in group II. The assessed features were PED (regular smooth or irregular flat), absence or presence of opaque material beneath flat PED, foveal thinning, disrupted outer retinal layers, choroidal excavation, subretinal deposits, sub-RPE deposits not related to PED, and increased choroidal thickness. Statistical analysis revealed that for group II, the total contribution of all studied features to CNV development was 65.6% in comparison to 11.1% of the contribution of the same factors to the CNV-free status in group I. Moreover, in group II, 3 major features were identified as statistically significant predictors for CNV development, namely, foveal thinning (75.0), presence of opaque material beneath flat PED (11.22), and increased choroidal thickness (7.84) (Table 3).

Table 3: Relative contribution (%) for studied chronic CSCR features in CNV development.

Feature	Group I (55 patients) = not complicated *N* (%)	Group II (5 patients) = complicated *N* (%)
RPED	9 (0.32)	0 (0.00)
IRPED	41 (2.02)	5 (0.66)
IRPED-T	12 (0.16)	0 (1.80)
IRPED-O	29 (1.02)	5 (11.22**)
FATR	11 (13.18**)	3 (75.00**)
DOLR	44 (3.03)	5 (0.45)
CEXC	1 (0.26)	0 (0.45)
SRD	35 (2.56)	4 (0.00)
SRPED-EF	30 (0.07)	5 (0.45)
CT	45 (1.23)	5 (7.84**)
Total relative contribution (%)	11.10	65.6

**Significant at 1%. CEXC: choroidal excavation; CT: choroidal thickness; DOLR: disrupted outer retinal layers; FT: foveal thinning; IRPED: irregular flat PED; IRPED-T: irregular flat PED with translucent (empty) sub-RPE space; IRPED-O: irregular flat PED with opaque (filled) sub-RPE space; RPED: regular smooth PED; SRD: subretinal deposits; SRPED-EF: sub-RPE deposits not related to irregular flat PED.

5. Case Reports

5.1. Case 1. A 52-year-old male has bilateral chronic CSCR of approximately 2-year duration. His BCVA was 1 logMAR and 0.2 logMAR in the right and left eyes, respectively. FFA of the right eye when he first presented during the acute attack showed typical smoke-stack appearance. As the chronic stage of the disease ensued, the fundus showed RPE pigmentary disturbance in the macular area along with subretinal deposits. On FFA, the old site of acute leakage demonstrated early pinpoint hyperfluorescence with increasing intensity through late frames suggestive of chronic point of leakage. The area of pigment epitheliopathy seen in the colored photo showed hyperfluorescence due to window defect. The corresponding SS-OCT scan of the macular area showed flat irregular PED and sub-RPE heterogeneous deposits. Subfoveal choroid was markedly thickened (737 μ). FFA and SS-OCT were inconclusive for the presence of CNV. SS-OCTA of the same eye clearly demonstrated the decorrelation signal characteristic of blood flow within an abnormal vascular network of active CNV (Figure 1). SS-OCTA of the left eye was normal.

5.2. Case 2. A 46-year-old male has bilateral chronic CSCR of approximately 1.5-year duration. His BCVA was 0.3 logMAR and 0.7 logMAR in the right and left eyes, respectively. Fundus examination of the left eye showed diffuse retinal pigment epitheliopathy in the macular area measuring approximately 5 disc diameters (DD) along with shallow neurosensory detachment. FFA of the same eye showed a large hyperfluorescent area caused by window defect that corresponds to the area of retinal pigment epitheliopathy seen in the colored photo. In addition, the macular area showed multiple hyperfluorescent leaking points that gradually increased in intensity throughout later phases with a typical inkblot pattern of leakage. SS-OCT of the same eye demonstrated neurosensory detachment along with subfoveal flat irregular PED associated with sub-RPE deposits and a single large regular smooth PED in the peripapillary area. Subfoveal choroid was thickened (455 μ) with markedly

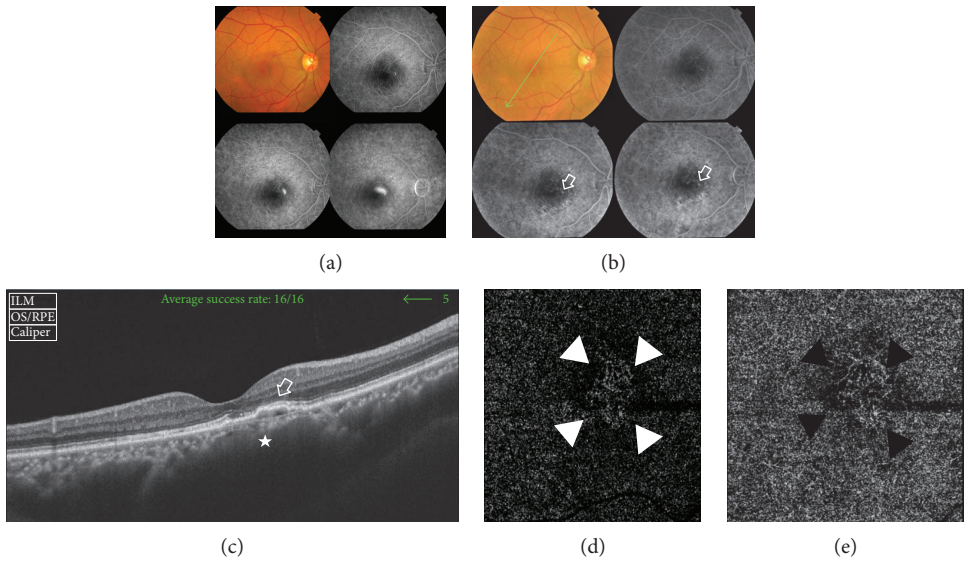

Figure 1: (a) The colored photo and FFA of the right eye of a 52-year-old male during acute CSCR. The macular area shows neurosensory detachment, measuring approximately 3 DD. Corresponding FFA shows a typical smoke-stack leaking pattern. (b) The colored photo and FFA of the same eye 2 years later. The posterior pole shows minimal retinal pigment disturbance in the inferior portion of the macular area along with subretinal deposits. On FFA, the old site of acute leakage demonstrates early pinpoint hyperfluorescence with increasing intensity through late frames suggestive of chronic point of leakage (open arrow). The area of pigment epitheliopathy seen in the colored photo shows hyperfluorescence due to window defect. (c) The corresponding SS-OCT image in a radial scan mode shows shallow PED with surface undulations and hyperreflective sub-RPE deposits (open arrow). There is associated disruption of ELM and IS/OS layers in the vicinity of the PED. Note the generalized dilatation of the choroidal vessels that is most marked in the area beneath the PED (star). Subfoveal choroidal thickness is 737 μ. (d) The en face SS-OCTA image of the same eye taken at the level of the outer retina in a 6 mm × 6 mm field. Note the hyperintense signal caused by increased blood flow within the vascular network of tiny interlacing capillaries (white arrow heads). The neovascular complex is surrounded by a hypointense hollow zone intervening between the lesion and the surrounding normal outer retina that generates a hypointense signal due to the absence of blood flow and is displayed as a dark-grey background. (e) The en face SS-OCTA image of the same lesion at the level of the choriocapillaris (black arrow heads).

dilated large choroidal vessels. FFA and SS-OCT were inconclusive for CNV formation. SS-OCTA of the left eye revealed the characteristic hyperintense signal of blood flow within the interlacing capillary network with looping and vascular anastomosis that was indicative of active CNV (Figure 2). SS-OCTA of the right eye was normal.

5.3. Case 3. A 40-year-old male has left chronic CSCR of approximately 1-year duration. His BCVA was 1 logMAR. The colored fundus photo of the left eye showed retinal pigment epitheliopathy in the macular area. FFA of the same eye showed hyperfluorescence due to a combination of window defect and multiple leaking points. SS-OCT of the same eye showed disruption of outer retinal layers with irregular flat PED formation and sub-RPE hyperreflective heterogeneous deposits and slightly thickened subfoveal choroid (315 μ). FFA and SS-OCT were inconclusive for CNV formation. SS-OCTA of the same eye showed the characteristic hyperintense signal of blood flow within the abnormal tiny capillary network that was indicative of active CNV formation (Figure 3).

5.4. Case 4. A 35-year-old male has left chronic CSCR of approximately 2-year duration. His BCVA was 0.5 logMAR. The colored photo of the left eye showed shallow neurosensory detachment in the macular area. SS-OCT of the same eye demonstrated subfoveal neurosensory detachment with subretinal deposits. In addition, there was flat irregular PED associated with sub-RPE hyperreflective amorphous material. Subfoveal choroid was thickened (400 μ). SS-OCTA of the same eye revealed the characteristic hyperintense signal of blood flow within the tiny interlacing capillary network that was indicative of active CNV (Figure 4).

5.5. Case 5. A 61-year-old male has bilateral chronic CSCR of approximately 2.5-year duration. His BCVA was 1.5 logMAR and 0.7 logMAR in the right and left eyes, respectively. The colored photo of the right eye showed a subretinal yellowish-white elevated lesion in the macular area, measuring approximately 2 DD and surrounded by subretinal hemorrhage. The posterior pole showed extensive retinal pigment epitheliopathy. On FFA, there were two distinct patterns of hyperfluorescence. The first pattern corresponded to the yellowish-white lesion seen in the colored photo and consisted of early hyperfluorescence that gradually increased in intensity due to pooling into PED. The second pattern consisted of early stippled hyperfluorescence that increased in intensity throughout the angiogram resulting in an ill-defined hyperfluorescent area. Other associated angiographic features were blocked fluorescence corresponding to subretinal hemorrhage and hyperfluorescence due to window defect corresponding to diffuse retinal pigment epitheliopathy. SS-OCT of the same eye demonstrated

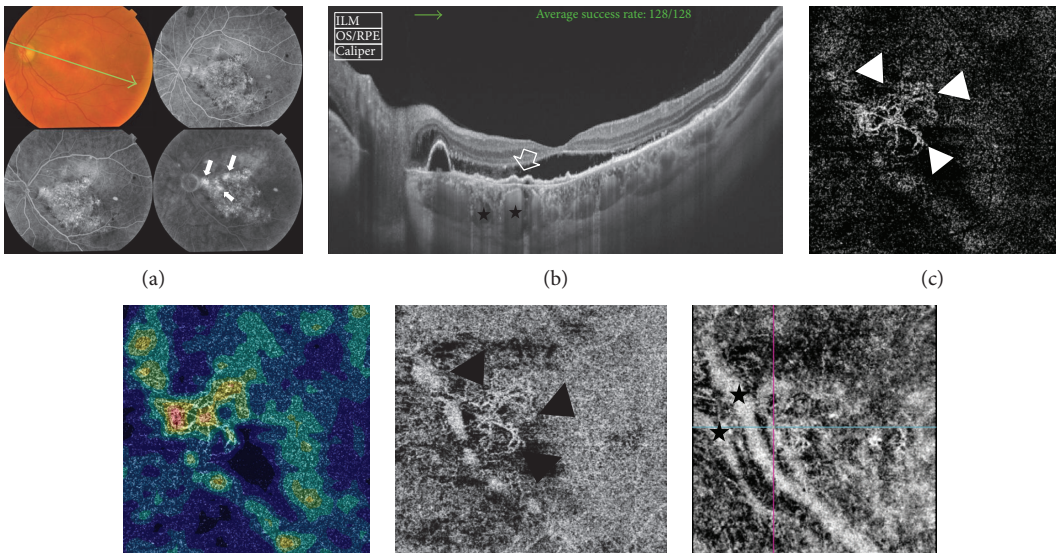

Figure 2: (a) The colored photo and FFA of the left eye of a 46-year-old male with bilateral chronic CSCR of approximately 1.5-year duration. The posterior pole shows diffuse retinal pigment epitheliopathy in the macular area measuring approximately 5 disc diameters (DD) in size along with shallow subretinal fluid and peripapillary PED. FFA shows a large hyperfluorescent area caused by window defect that corresponds to the area of retinal pigment epitheliopathy seen in the colored photo. In addition, the macular area shows multiple hyperfluorescent leaking points that gradually increase in intensity throughout later phases with a typical inkblot pattern of leakage (arrows). (b) SS-OCT image. A 12.0 mm radial scan is selected to include the peripapillary area. The scan shows subfoveal neurosensory detachment extending to the peripapillary area, which is associated with subretinal deposits. A single large regular smooth PED is seen in the peripapillary area. A subfoveal shallow PED with an undulating thickened surface and sub-RPE hyperreflective amorphous deposits is shown (open arrow). The subfoveal choroidal vessels are engorged (black stars). Subfoveal choroid thickness is 455 μ. (c) The en face SS-OCTA image of the same eye taken at the level of the outer retina in a 4.5 mm × 4.5 mm field. Note the hyperintense signal caused by increased blood flow within the CNV complex. The complex is composed of a network of tiny arborizing capillaries with frequent anastomosis and looping in the periphery of the lesion (white arrow heads). (d) The corresponding color-coded density map reflecting blood flow at the level of the outer retina. Note the entire background has variable shades of blue typical of avascular outer retina. The CNV complex stands out with its bright red signal indicating dense blood flow. (e) The en face SS-OCTA image of the same lesion at the level of the choriocapillaris (black arrow heads). (f) The en face SS-OCTA image after manual adjustment of the segmentation slab to a deeper position into the choroid to demonstrate two abnormally dilated choroidal vessels corresponding to increased subfoveal choroidal thickness on SS-OCT (black stars).

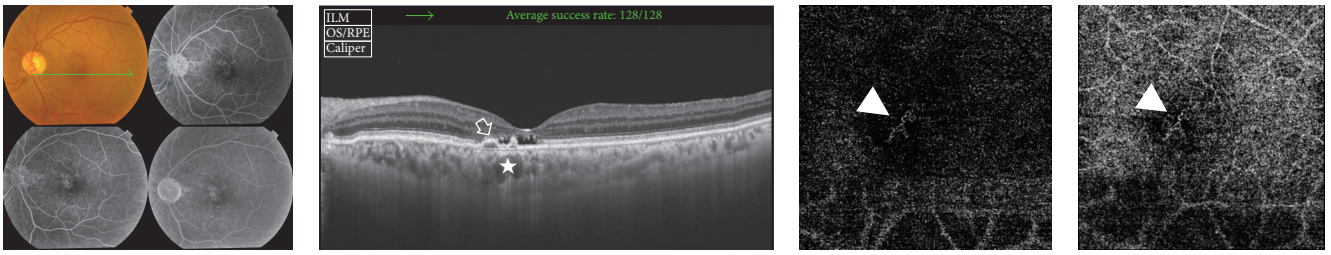

Figure 3: (a) The colored photo and FFA of the left eye of a 40-year-old male with left chronic CSCR of approximately 1-year duration. The posterior pole shows retinal pigment epitheliopathy in the macular area. FFA of the same eye shows multiple hyperfluorescent leaking points in the macular area that gradually increase in intensity throughout later phases resulting in a diffuse ill-defined hyperfluorescence pattern. (b) The corresponding SS-OCT image in a radial scan mode shows subfoveal shallow neurosensory detachment with subretinal deposits and associated disruption of ELM and IS/OS layers. Note the double-humped irregular PED in the parafoveal area with underlying opaque hyperreflective material (open arrow). The choroid vessels underneath the PED are engorged (star). Subfoveal choroidal thickness is 315 μ. (c) The *en face* SS-OCTA image of the same eye taken at the level of the outer retina in a 6 mm × 6 mm field. Note the hyperintense signal caused by increased blood flow within the CNV complex composed of tiny intertwining vascular loops (arrow head). (d) The en face SS-OCTA image of the same lesion at the level of the choriocapillaris.

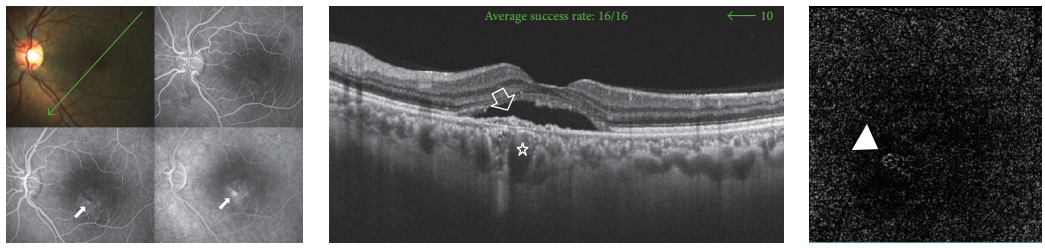

(a) (b) (c)

Figure 4: (a) The colored photo and FFA of the left eye of a 35-year-old male with chronic CSCR of approximately 2-year duration. The macular area shows shallow neurosensory detachment. Corresponding FFA shows hyperfluorescent leaking points (arrows). (b) The radial scan SS-OCT image of the same eye demonstrates subfoveal neurosensory detachment with subretinal hyperreflective deposits. A subfoveal flat irregular PED associated with sub-RPE hyperreflective material is seen (open arrow). Subfoveal choroidal thickness is 400 μ. Note the engorged choroidal vessels beneath the PED (star). (c) The en face SS-OCTA image of the same eye at the level of the outer retina in a 4.5 mm × 4.5 mm field. Note the characteristic hyperintense signal of vascular flow within tiny interlacing capillaries in the foveal area (arrow head).

neurosensory detachment along with subretinal hyperreflective heterogeneous material, sizeable subfoveal PED, and sub-RPE hyperreflective material. The blocking effect of significant hemorrhage hindered exclusion of CNV formation using FFA and SS-OCT alone. SS-OCTA of the right eye revealed the characteristic hyperintense signal of a subfoveal neovascular complex composed of a main trunk with branching smaller vessels each terminating in polyp-like configuration reminiscent of PCV. In addition, there was another juxtapapillary larger neovascular complex composed of dense capillary arborization and feeder vessels (Figure 5). SS-OCTA of the left eye was normal.

6. Discussion

Choroidal neovascular membrane masquerading as chronic CSCR is an uncommon yet devastating complication that eventually leads to irreversible visual loss [10, 11, 24]. Therefore, early detection of CNV arising on top of chronic CSCR is pivotal in establishing the diagnosis and prompt initiation of therapy for vision salvage in those patients. Particularly, type 1 variant of CNV can present a diagnostic predicament using conventional imaging modalities [13–16].

In the current series, we combined SS-OCTA with SS-OCT and FFA for the detection of CNV in chronic CSCR cases. Our results revealed the presence of type 1 CNV in 8.3% of the study population, of which one eye developed PCV. This finding is comparable with that of Hage et al. [14] who reported a 5.8% incidence of type 1 CNV in a retrospective case series of 172 eyes. Similarly, a prospective observational cross-sectional study including 27 eyes with chronic CSCR by Filho et al. [23] detected CNV secondary to chronic CSCR in 8 out of 27 eyes (30%). Four eyes had type 1 CNV, whereas four eyes developed type 1 and type 2 mixed variant. El-Maftouhi et al. [13] reported a 58% incidence of CNV secondary to chronic CSCR. De Carlo et al. [11] detected CNV in 28.5% of 49 eyes with chronic CSCR. Our finding is further corroborated by two other series by Yannuzzi et al. [12] and Fung et al. [10] and a case report by Yang et al. [15] who detected CNV secondary to chronic CSCR. These authors used multimodal imaging exclusive of OCTA and reported type 1 CNV and its variant PCV either masquerading as chronic CSCR at presentation or developing over the course of follow-up.

The current study focused on the analysis of several characteristic features of chronic CSCR (Table 2) and their correlation with the development of CNV. Our results revealed 3 statistically significant major predictors in SS-OCT images for progression to neovascularization, namely, foveal thinning, presence of opaque material beneath irregular flat PED, and increased choroidal thickness. Accordingly, we could propose a high-risk profile of chronic CSCR for progression to type 1 CNV formation. In accordance with our findings, Hage et al. [14] detected the presence of flat irregular PED in all eyes with chronic CSCR that developed CNV. The authors coined the terms "optically filled" and "not optically filled" to describe OCT findings of the amorphous contents of the sub-RPE space beneath the PED. All eyes with CNV in their series had an optically filled sub-RPE space. Similarly, De Carlo et al. [11] classified patients into two groups: those with regular PED and those with irregular PED. The authors stated that the presence of irregular flat PED in chronic CSCR is a statistically significant risk factor for the development of CNV. The authors however did not correlate the content of the sub-RPE space with CNV in their results. Instead, they studied the relation between PED and sub- or intraretinal fluid and concluded that the presence or absence of fluid was not helpful in predicting the development of CNV in chronic CSCR. Our findings regarding increased choroidal thickness in patients with chronic CSCR are consistent with those of the published literature that corroborate the choroidal vascular hyperpermeability theory as the main etiological factor of the disease [5, 6, 25–27]. Moreover, in our series, increased choroidal thickness was a statistically significant contributing factor in the development of CNV in the 5 cases reported herein. In one of our cases (Figure 2), we were able to demonstrate a marked increase in the caliber of choroidal vessels using SS-OCTA projection of large choroidal vessels that corresponded to subfoveal increased choroidal thickness in SS-OCT. In accordance with our findings, El-Maftouhi et al. [13] found that all eyes, which developed CNV in chronic CSCR, had associated

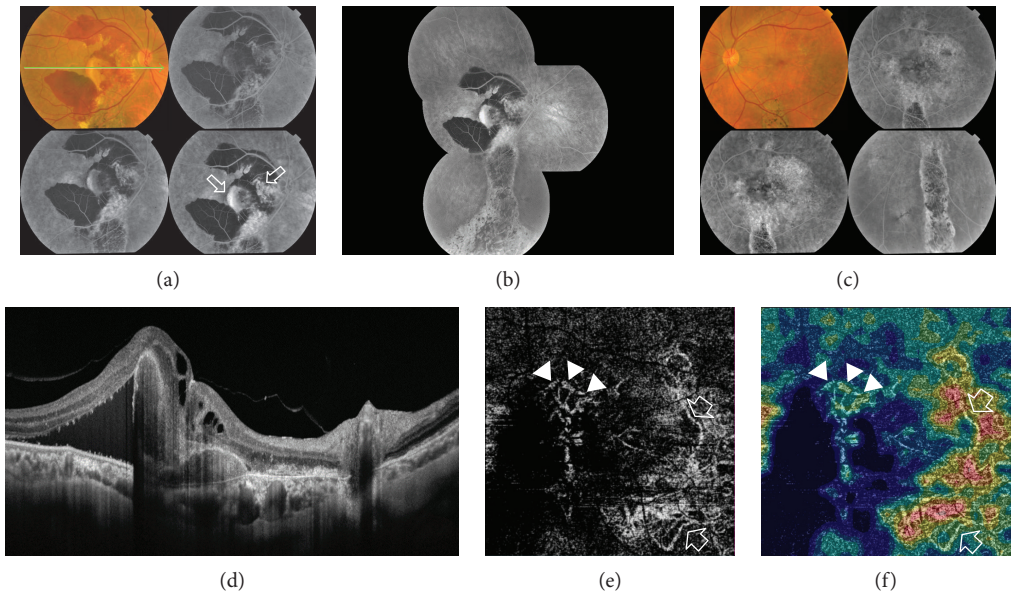

Figure 5: (a) The colored photo and FFA of the right eye of a 61-year-old male with bilateral chronic CSCR of approximately 2.5-year duration. The posterior pole shows a subretinal yellowish-white elevated lesion in the macular area measuring approximately 2 DD. The lesion is surrounded by extensive subretinal hemorrhage that extends beyond the temporal vascular arcades. On FFA, there were two distinct patterns of hyperfluorescence. The first pattern corresponded to the yellowish-white lesion seen in the colored photo and consisted of early hyperfluorescence that gradually increased in intensity due to pooling into PED. The second pattern consisted of early stippled hyperfluorescence that increased in intensity throughout the angiogram resulting in an ill-defined hyperfluorescent area (open arrows). Note the blocked fluorescence corresponding to subretinal hemorrhage in the colored photo. (b) The composite FFA of the right eye shows extensive retinal pigment epitheliopathy in the macular area, extending inferiorly due to gravitation of subretinal fluid giving rise to the characteristic teardrop sign (atrophic RPE track). (c) The colored photo and FFA of the left eye showing diffuse retinal pigment epitheliopathy and the characteristic teardrop sign. (d) The radial scan SS-OCT of the right eye demonstrates neurosensory detachment along with subretinal hyperreflective heterogeneous material, sizeable subfoveal PED, and sub-RPE hyperreflective material. (e) The SS-OCTA of the right eye at the level of the outer retina in a 4.5 mm × 4.5 mm field revealed the characteristic hyperintense signal of a subfoveal neovascular complex composed of a main trunk with branching smaller vessels each terminating in polyp-like configuration reminiscent of PCV (arrow heads). In addition, there was another juxtapapillary larger neovascular complex composed of dense capillary arborization. At least two feeder vessels could be identified (open arrows). (f) The corresponding color-coded density map reflecting blood flow at the level of the outer retina. Note the intense red signal denoting high flow within the neovascular complexes seen, contrasting with the blue background typical of avascular outer retina.

choroidal vascular hyperpermeability on ICG angiography, whereas all eyes that did not develop CNV had normal choroidal circulation. Similarly, Yang et al. [16] in a prospective series including 68 eyes with CSCR reported mean subfoveal choroidal thickness of 478 μ. It is worthy of note that in the current study, we detected increased choroidal thickness in the normal fellow eye of those patients who had unilateral chronic CSCR, though to a lesser extent than that in the affected eye (412 μ versus 354 μ). This finding is congruous with that of the study of Kim et al. [28] who reported increased choroidal thickness of unaffected eyes in patients with unilateral CSCR.

The important limitation of the current study is the lack of comparison between SS-OCTA and ICG angiography in assessing the choroidal circulation particularly that increased choroidal thickness is one of the 3 major predictors of progression to CNV formation according to our results. However, evidence from the literature supports the notion that increased choroidal thickness by SS-OCT is equivalent to choroidal vascular hyperpermeability [25] and that SS-OCTA projection of choroidal circulation corresponds to ICG in the evaluation of choroidal blood flow in patients with CSCR [29]. Another limitation is that the current study did not include a concurrent comparison group that included patients with chronic CSCR subjected to treatment with PDT and/or anti-VEGF agents. Comparing both groups would reveal important insights into the progression of chronic CSCR to CNV formation and the effect of treatment on the alteration of the high-risk chronic CSCR profile we proposed in the current study.

7. Conclusion

Silent type 1 CNV is an established complication of chronic CSCR. The presence of foveal thinning, irregular flat RPE associated with sub-RPE deposits, and increased choroidal thickness represents a high-risk profile that warrants exclusion of CNV formation using multimodal imaging protocol in which SS-OCTA is an integral component alongside conventional FFA and SS-OCT, particularly when both reveal inconclusive results. A combination of SS-OCT and SS-OCTA is a risk-free analogue to FFA in clinical situations where the latter is contraindicated.

Conflicts of Interest

None of the authors have proprietary interest in any material used in this study.

References

[1] C. Prünte and J. Flammer, "Choroidal capillary and venous congestion in central serous chorioretinopathy," *American Journal of Ophthalmology*, vol. 121, no. 1, pp. 26–34, 1996.

[2] R. F. Spaide and E. H. Ryan, "Loculation of fluid in the posterior choroid in eyes with central serous chorioretinopathy," *American Journal of Ophthalmology*, vol. 160, no. 6, pp. 1211–1216, 2015.

[3] B. Nicholson, J. Noble, F. Forooghian, and C. Meyrele, "Central serous chorioretinopathy: update on pathophysiology and treatment," *Survey of Ophthalmology*, vol. 58, no. 2, pp. 103–126, 2013.

[4] C. Yun, J. Oh, J. Y. Han, S. Y. Hwang, S. W. Moon, and K. Huh, "Peripapillary choroidal thickness in central serous chorioretinopathy. Is choroid outside the macula also thick?," *Retina*, vol. 35, no. 9, pp. 1860–1866, 2015.

[5] S. Kuroda, Y. Ikuno, Y. Yasuno et al., "Choroidal thickness in central serous chorioretinopathy," *Retina*, vol. 33, no. 2, pp. 302–308, 2013.

[6] Y. Imamura, T. Fujiwara, R. Margolis, and R. F. Spaide, "Enhanced depth imaging optical coherence tomography of the choroid in central serous chorioretinopathy," *Retina*, vol. 29, no. 10, pp. 1469–1473, 2009.

[7] D. T. Liu, A. C. Fok, W. Chan, T. Y. Lai, and D. S. Lam, "Central serous chorioretinopathy," in *Retina*, S. J. Ryan, A. P. Schachat and S. R. Sadda, Eds., vol. 2pp. 1291–1305, Saunders, Philadelphia (PA), 2013.

[8] J. D. M. Gass, "Diseases causing choroidal exudative and hemorrhagic localized (disciform) detachment of the retina and retinal pigment epithelium," in *Stereoscopic Atlas of Macular Diseases. Diagnosis and Treatment*, pp. 49–285, Mosby, St. Louis, 1997.

[9] S. M. McClintic, Y. Jia, D. Huang, and S. T. Bailey, "Optical coherence tomography angiography of choroidal neovascularization associated with central serous chorioretinopathy," *JAMA Ophthalmology*, vol. 133, no. 10, pp. 1212–1214, 2015.

[10] A. T. Fung, L. A. Yannuzzi, and K. B. Freund, "Type I (sub-retinal pigment epithelial) neovascularization in central serous chorioretinopathy masquerading as neovascular age-related macular degeneration," *Retina*, vol. 32, no. 9, pp. 1829–1837, 2012.

[11] T. E. De Carlo, A. Rosenblatt, M. Goldstein, C. R. Baumal, A. Loewenstein, and J. S. Duker, "Vascularization of irregular retinal pigment epithelial detachments in chronic central serous chorioretinopathy evaluated with OCT angiography," *Ophthalmic Surgery, Lasers and Imaging Retina*, vol. 47, no. 2, pp. 128–133, 2016.

[12] L. A. Yannuzzi, K. B. Freund, M. Goldbaum et al., "Polypoidal choroidal vasculopathy masquerading as central serous chorioretinopathy," *Ophthalmology*, vol. 107, no. 4, pp. 767–777, 2000.

[13] M. Q. El-Maftouhi, A. El Maftouhi, and C. M. Eandi, "Chronic central serous chorioretinopathy imaged by optical coherence tomographic angiography," *American Journal of Ophthalmology*, vol. 160, no. 3, pp. 581–587.e1, 2015.

[14] R. Hage, S. Mrejen, V. Krivosic, G. Quentel, R. Tadayoni, and A. Gaudric, "Flat irregular retinal pigment epithelium detachments in chronic central serous chorioretinopathy and choroidal neovascularization," *American Journal of Ophthalmology*, vol. 159, no. 5, pp. 890–903.e3, 2015.

[15] L. H. Yang, J. B. Jonas, and W. B. Wei, "Conversion of central serous chorioretinopathy to polypoidal choroidal vasculopathy," *Acta Ophthalmologica*, vol. 93, no. 6, pp. e512–e514, 2015.

[16] L. Yang, J. B. Jonas, and W. Wenbin, "Optical coherence tomography-assisted enhanced depth imaging of central serous chorioretinopathy," *Investigative Ophthalmology & Visual Science*, vol. 54, no. 7, pp. 4659–4665, 2013.

[17] P. E. Stanga, E. Tsamis, A. Papayannis, F. Stringa, T. Cole, and A. Jalil, "Swept-source optical coherence tomography angiography™ (Topcon Corp, Japan): technology review," *Developments in Ophthalmology*, vol. 56, pp. 13–17, 2016.

[18] S. Bonnin, V. Mané, A. Couturier et al., "New insight into the macular deep vascular plexus imaged by optical coherence tomography angiography," *Retina*, vol. 35, no. 11, pp. 2347–2352, 2015.

[19] I. Grulkowski, J. J. Liu, B. Potsaid et al., "Retinal, anterior segment and full eye imaging using ultrahigh speed swept source OCT with vertical-cavity surface emitting lasers," *Biomedical Optics Express*, vol. 3, no. 11, pp. 2733–2751, 2012.

[20] S. S. Gao, G. Liu, D. Huang, and Y. Jia, "Optimization of the split-spectrum amplitude-decorrelation angiography algorithm on a spectral optical coherence tomography system," *Optics Letters*, vol. 40, no. 10, pp. 2305–2308, 2015.

[21] L. Kuehlewein, T. C. Tepelus, L. An, M. K. Durbin, S. Srinivas, and S. R. Sadda, "Noninvasive visualization and analysis of the human parafoveal capillary network using swept source OCT optical microangiography," *Investigative Ophthalmology & Visual Science*, vol. 56, no. 6, pp. 3984–3988, 2015.

[22] M. C. Savastano, B. Lumbroso, and M. Rispoli, "In vivo characterization of retinal vascularization morphology using optical coherence tomography angiography," *Retina*, vol. 35, no. 11, pp. 2196–2203, 2015.

[23] M. A. B. Filho, T. E. De Carlo, D. Ferrara et al., "Association of choroidal neovascularization and central serous chorioretinopathy with optical coherence tomography angiography," *JAMA Ophthalmology*, vol. 133, no. 8, pp. 899–906, 2015.

[24] D. Ferrara, K. J. Mohler, N. Waheed et al., "En face enhanced-depth swept-source optical coherence tomography features of chronic central serous chorioretinopathy," *Ophthalmology*, vol. 121, no. 3, pp. 719–726, 2014.

[25] I. Maruko, T. Iida, Y. Sugano, A. Ojima, and T. Sekiryu, "Subfoveal choroidal thickness in fellow eyes of patients with central serous chorioretinopathy," *Retina*, vol. 31, no. 8, pp. 1603–1608, 2011.

[26] I. Maruko, T. Iida, Y. Sugano, A. Ojima, M. Ogasawara, and R. F. Spaide, "Subfoveal choroidal thickness after treatment of central serous chorioretinopathy," *Ophthalmology*, vol. 117, no. 9, pp. 1792–1799, 2010.

[27] S. Razavi, E. H. Souied, E. Cavallero, M. Weber, and G. Querques, "Assessment of choroidal topographic changes by swept source optical coherence tomography after photodynamic therapy for central serous chorioretinopathy," *American Journal of Ophthalmology*, vol. 157, no. 4, pp. 852–860, 2014.

[28] Y. T. Kim, S. W. Kang, and K. H. Bai, "Choroidal thickness of both eyes of patients with unilaterally active central serous chorioretinopathy," *Eye*, vol. 25, no. 12, pp. 1635–1640, 2011.

[29] M. M. Teussink, M. B. Breukink, M. J. J. P. Van Grinsven et al., "OCT angiography compared to fluorescein and indocyanine green angiography in chronic central serous chorioretinopathy," *Investigative Ophthalmology & Visual Science*, vol. 56, no. 9, pp. 5229–5237, 2015.